Changing effects of external forcing on Atlantic-Pacific interactions

Soufiane Karmouche[1,2], Evgenia Galytska[1,2], Gerald A. Meehl[3], Jakob Runge[4,5], Katja Weigel[1,2], and Veronika Eyring[2,1]

[1]University of Bremen, Institute of Environmental Physics (IUP), Bremen, Germany
[2]Deutsches Zentrum für Luft- und Raumfahrt e.V. (DLR), Institut für Physik der Atmosphäre, Oberpfaffenhofen, Germany
[3]Climate and Global Dynamics Laboratory, National Center for Atmospheric Research (NCAR), Boulder, CO, USA
[4]Deutsches Zentrum für Luft- und Raumfahrt e.V. (DLR), Institut für Datenwissenschaften, Jena, Germany
[5]Fachgebiet Klimainformatik, Technische Universität Berlin, Berlin, Germany

Correspondence: Soufiane Karmouche (sou_kar@uni-bremen.de)

Abstract. Recent studies have highlighted the increasingly dominant role of external forcing in driving Atlantic and Pacific Ocean variability during the second half of the ~~20th~~ 20th century. This paper provides insights into the underlying mechanisms driving interactions between modes of variability over the two basins. We define a set of possible drivers of these interactions and apply causal discovery to reanalysis data, ~~an ensemble~~ two ensembles of pacemaker simulations where ~~the observed El Niño Southern Oscillation (ENSO) is prescribed~~sea surface temperatures in either the tropical Pacific or the North Atlantic are nudged to observations, and a pre-industrial control ~~simulation~~run. We also utilize large ensemble means of historical simulations from the Coupled Model Intercomparison Project Phase 6 (CMIP6) to quantify the effect of external forcing and improve the understanding of its impact. ~~By conducting a~~ A causal analysis of the historical time series ~~,~~ between 1950 and 2014 identifies a regime switch ~~is identified~~ in the interactions between major modes of Atlantic and Pacific climate variability ~~. Causal networks derived from pacemaker simulationssupport this finding and further demonstrate that the effect of external forcing could favor an Atlantic-driven regime between 1985 and 2014~~ in both reanalysis and pacemaker simulations. A sliding window causal analysis reveals a decaying ENSO effect on the Atlantic as the North Atlantic fluctuates towards an anomalously warm state. The causal networks also demonstrate that external forcing contributed to strengthening the Atlantic's negative-sign effect on ENSO since the mid-1980s where warming tropical ~~North~~ Atlantic sea surface temperatures induce a La Niña-like cooling in the equatorial Pacific during the following season through ~~a strengthening~~ an intensification of the Pacific Walker ~~Circulation. This negative sign effect was~~ circulation. The strengthening of this effect is not detected when the historical external forcing signal is removed in the Pacific pacemaker ensemble. The analysis of the pre-industrial control run ~~further~~ supports the notion that the Atlantic and Pacific modes of natural climate variability exert contrasting impacts on each other even in the absence of ~~external forcing.~~ anthropogenic forcing. The interactions are shown to be modulated by the (multi)decadal states of temperature anomalies of both basins with stronger connections when these states are "out of phase". We show that causal discovery can ~~quantify previously unknown connections and thus~~ detect previously documented connections and provides important potential ~~to~~ for a deeper understanding of the mechanisms driving changes in regional and global climate variability.

1 Introduction

One of the biggest challenges in climate science is associated with disentangling the effects of internal climate variability and external forcings and robust quantification of their impacts. External forcing includes changes to the climate system caused by natural factors such as volcanic eruptions, solar radiation, or from the human emission of greenhouse gas (GHG) and aerosols. Internal climate variability, on the other hand, refers to the inherent fluctuations in the climate system that arise from complex interactions between the atmosphere, oceans, land, and cryosphere (Masson-Delmotte et al., 2023). For instance, the interactions between the ocean and atmosphere produce unique patterns of variability at different time scales, such as El Niño-Southern Oscillation (ENSO, Bjerknes, 1966; BJERKNES, 1969; Neelin et al., 1998), Pacific Decadal Variability (PDV, Mantua et al., 1997; Newman et al., 2016), and Atlantic Multidecadal Variability (AMV, Trenberth and Shea, 2006; Zhang et al., 2019). Despite the considerable advancements through different phases of the Coupled Model Intercomparison Project (CMIP), including the ability to represent the statistical properties and spatial patterns of modes of climate variability, accurately simulating them as in the observed record still poses daunting challenges (Eyring et al., 2019; Fasullo et al., 2020; Karmouche et al., 2023). In addition to the short historical record, the intricate nature of the climate system and the non-linear characteristics of natural climate variability impose inherent limitations on predictability and introduce inseparable uncertainty into climate model projections (Deser et al., 2010; Meehl et al., 2013; Fasullo et al., 2020; Eyring et al., 2021; Deser and Phillips, 2023). This underlines the importance of studying natural climate variability modes and their teleconnections to advance our understanding of the climate system and improve the reliability of climate model projections (Deser and Phillips, 2023).

Previous studies have explored connections between the Atlantic and Pacific basins, focusing on the influence of the Walker circulation (BJERKNES, 1969) on both interannual and decadal timescales (Latif and Grötzner, 2000; McGregor et al., 2014; Meehl et al., 2016; Ruprich-Robert et al., 2017; Meehl et al., 2020). Other studies found that the Atlantic drives the Pacific, while the Pacific can also drive the Atlantic, and there are influences between the two through the tropical Indian Ocean (Kumar et al., 2013; Li et al., 2015; Ruprich-Robert et al., 2017; Levine et al., 2017; Meehl et al., 2016; Yang et al., 2019; An et al., 2021). For example, on the decadal timescale, Meehl et al. (2020) demonstrate how a positive AMV can lead to a negative PDV through anomalous Walker circulation. They showed that a negative PDV, which triggers a same-sign response in the tropical Atlantic, contributes to AMV's transition from a positive to a negative phase (Fig. 3 in Meehl et al., 2020). The study highlights that in addition to the tropical Walker circulation~~(BJERKNES, 1969)~~, positive convective heating and precipitation anomalies in the tropical Pacific can establish connections to extra-tropical modes of atmospheric variability, e.g. the Pacific-North American pattern (PNA) and Pacific South American pattern (PSA), which also contribute to the same-sign effect of the Pacific on the Atlantic. The tropical pathway connecting the Pacific and the Atlantic happens mainly through modifications to the Walker circulation affecting large-scale tropical weather systems. On the other hand, the extratropical southern hemisphere (through the PSA) and northern hemisphere teleconnections illustrated through the PNA and North Atlantic Oscillation (NAO, Barnett, 1985; Brönnimann et al., 2006; Scaife et al., 2014) ~~,~~not only connect the Atlantic-Pacific basins but also play important roles in modulating Arctic sea ices responses (Polyakov and Johnson, 2000; Meehl et al., 2018; Galytska et al., 2022) and

shaping European climate (Brönnimann et al., 2006; Brönnimann, 2007). ~~On the seasonal and interannual timescales, a study by Park et al. (2023b) on inter-basin interactions~~

Similar to the connection between AMV and PDV, previous research revealed well-established contrasting responses between the Atlantic and Pacific ~~Oceans showed that ENSO affects~~ tropical sea surface temperature ~~anomalies (SSTAs) of the Tropical North Atlantic (TNA)~~ SST) also on the interannual timescale (Zebiak, 1993; Latif and Grötzner, 2000; Ham et al., 2013b; Martín-
. At the equator, ENSO contributes to the Atlantic Zonal Mode (AZM), also known as the Atlantic Niño, through the Walker circulation (Saravanan and Chang, 2000; Sutton et al., 2000; Wang, 2019). On the other hand, it is suggested that an Atlantic Niño, peaking during the boreal summer upwelling season, can induce a La Niña event in the Pacific during the following winter through an atmospheric bridge altering the Walker circulation (Ham et al., 2013b, a; Martín-Rey et al., 2014a; Keenlyside et al., 2013)
. ENSO is also related to the second mode of tropical Atlantic variability, known as the Atlantic Meridional Mode (AMM), expressed as a cross-equatorial SST gradient with opposite signs between the tropical South Atlantic (TSA) and the tropical North Atlantic (TNA, Rajagopalan et al., 1998; Enfield et al., 1999; Chiang and Vimont, 2004). Both AZM and AMM are linked to changes in the Intertropical Convergence Zone (ITCZ) and associated winds (Masson-Delmotte et al., 2023). Several studies show that ENSO affects north tropical Atlantic SST anomalies (SSTAs) during the spring and summer through tropical and extratropical pathways ~~(also discussed in Meehl et al., 2016, 2020)~~(Enfield and Mayer, 1997; Klein et al., 1999; Saravanan and Chang, 2000
. Conversely, SST variability ~~of TNA~~ in the tropical Atlantic can also influence an ENSO event during the following boreal winter by modifying anomalous low-level zonal winds through atmospheric teleconnections over the equatorial western Pacific ~~(Park and Li, 2018; Park et al., 2023b). The high~~ (Ham et al., 2013b; Park and Li, 2018; Park et al., 2023b). In addition to ENSO, NAO also contributes to forcing SSTAs in the TNA region (Czaja et al., 2002; Visbeck et al., 2003). The weak intensity of the subtropical high during a negative NAO phase weakens the northeasterly winds, which favors TNA warming. The high SSTAs in the ~~tropical Atlantic~~ TNA region trigger an atmospheric response that strengthens the connection between TNA and ENSO (Wang et al., 2017b; Park et al., 2019). The impact of the ~~TNA~~ Atlantic on ENSO, which has become more significant since the mid-1980s is associated with an increase in the climatological mean SST in the ~~tropical~~ North Atlantic, which can be attributed to a positive phase shift of AMV and/or human-caused warming ~~(Park and Li, 2018; Meehl et al., 2020; Park et al., 2023b)~~ (Park and Li, 2018; Yang et al., 2021; Meehl et al., 2020; Park et al., 2023b). In turn, the effect of ENSO on TNA has decreased since the mid-1980s, supporting the existence of two regimes of contrasting responses as proposed by ~~(Meehl et al., 2020)~~ Meehl et al. (2020) and described by Park et al. (2023b) as a Pacific-driven regime (1950 to mid-1980s) as opposed to an Atlantic-driven regime (from mid-1980s to 2014), where both span over multiple decades.

While ~~the~~ debate over the precise attribution of ~~recent warming trends~~ the early-2000s warming slowdown and the mid-1980s regime switch is still ongoing, it is evident that signals from natural internal variability, GHG-induced warming, and aerosol-cooling all play roles in the observed changes in global temperature variability over the historical record (Brönnimann, 2007; Meehl et al., 2013; Kosaka and Xie, 2013; Dong et al., 2014; Mann et al., 2014; McGregor et al., 2014; Li et al., 2015; Meehl et al., 2016; Kucharski et al., 2015; Smith et al., 2016; Dong and McPhaden, 2017; Haustein et al., 2019). There is growing evidence, however, that in the Atlantic, external forcing is responsible for the recent AMV changes and its widespread impacts (Murphy et al., 2017; Klavans et al., 2022; He et al., 2023). In addition to that, ~~differences in the considered timescales~~

and limited coverage of the in-situ observations over the tropical Pacific contribute contributes to a lack of consensus between among previous studies on the reasons behind the recently observed 1979-2014 strengthening of the Walker circulation (Vecchi and Soden, 2007; Power and Kociuba, 2011; L'Heureux et al., 2013; DiNezio et al., 2013; Kociuba and Power, 2014). Findings from Chung et al. (2019) indicate that internal variability linked to the Interdecadal Pacific Oscillation (IPO, similar to PDV) likely played the dominant role in the recent strengthening of the Walker circulation. Other studies, however, emphasize the role of SST variability in neighboring ocean basins, such as the Atlantic (Kucharski et al., 2011; McGregor et al., 2014) and/or the Indian Ocean (Luo et al., 2012), in modulating the tropical Pacific variability. This means that the anthropogenic contribution to the Atlantic SST warming during the recent decades (Watanabe and Tatebe, 2019; Klavans et al., 2022) might have influenced the Pacific variability and its effect on the recent strengthening of the Walker circulation.

To address the effects of a changing climate on the interactions between these modes, it is necessary to isolate internal variability from external forcing. While the "signal-to-noise paradox" in climate models is still a topic of debate (Scaife et al., 2014; Wang et al., 2017a; Sato et al., 2018; Smith et al., 2019; Chylek et al., 2020; Klavans et al., 2021, 2022), the use of large ensemble simulations has been proven to be extremely helpful to capture the observed trends and to help the detection and attribution of anthropogenic climate change in the observational record (Meehl et al., 2013; Menary et al., 2020; Borchert et al., 2021; Deser, 2020; Tebaldi et al., 2021; Klavans et al., 2022; Deser and Phillips, 2023). Studies proved that large ensembles can provide a robust sampling of models' internal variability and help assess externally forced changes in the characteristics of simulated internal variability (Menary et al., 2020; Borchert et al., 2021; Klavans et al., 2022; Deser and Phillips, 2023). Therefore, this paper utilizes large ensembles from CMIP Phase 6 historical simulations (CMIP6, Eyring et al., 2016) to represent all historical natural and human-induced external forcing.

Beyond mere correlation, causal discovery aims to learn the underlying causes and effects of the climate system (Runge et al., 2023). Similar to our previous research (Karmouche et al., 2023), in this study we apply a causal discovery algorithm to understand the regime-dependent causal networks connecting coupled and atmospheric modes of climate variability over the Atlantic and Pacific. While Karmouche et al. (2023) addressed teleconnections happening at yearly-interannual to decadal lags, this paper focuses on the seasonal to interannual timescale. The study encompasses a causal analysis of reanalysis data to investigate the distinctive regimes of teleconnections during two historical periods as suggested by Meehl et al. (2020); Park et al. (2023b), namely the Pacific-driven regime (1950-1983) and the Atlantic-driven regime (1985-20141983-2014). Pacemaker simulations are also used to explore the role of ENSO on North Pacific roles of ENSO and North Atlantic teleconnections SSTAs in the cross-basin interactions before and after removing the externally forced signal. Finally, to show that Atlantic-Pacific interactions happen naturally, even in the absence of external human influences, we show results using a pre-industrial control run.

2 Data

2.1 ~~Observational and~~ Observational and reanalyses datasets

To calculate SST-based indices over the Atlantic and Pacific during the observed historical 1950-2014 period, we use the Hadley Centre Sea Ice and Sea Surface Temperature (HadISST, Rayner et al., 2003) dataset. We also use sea level pressure (SLP) and zonal wind component (U) at 925 hPa obtained from the National Center for Environmental Prediction-National Center for Atmospheric Research reanalysis 1 dataset (NCEP-NCAR-R1 Kalnay et al., 1996) to calculate indices for the atmospheric modes (NAO and PNA) and the Pacific Walker ~~Circulation~~ circulation (PWC).

2.2 ~~Pacific pacemaker~~ Pacemaker simulations

To address the effect of external forcing on the Atlantic-Pacific interactions, we utilized a 10-member ensemble of the Community Earth System Model 2 (CESM2; Danabasoglu et al., 2020) in which SSTAs in the eastern tropical Pacific were nudged to National Oceanic and Atmospheric Administration (NOAA) Extended Reconstruction Sea Surface Temperature version 5 (ERSSTv5) data during 1880-2019. Similar to the reanalyses datasets (see Sect. 2.1), the analysis of Pacific pacemaker simulations focuses on the period from 1950 to 2014. To preserve the mean state and biases of the model, the SST nudging was only applied to the anomalies, not the total SST. The ensemble includes all CMIP6 time-varying external, natural, and anthropogenic forcings, using historical forcings prior to 2014 and SSP3-7.0 forcing thereafter. ~~Similarly to reanalysis data, we~~ We extract surface temperature (TS), SLP, and U variables from this dataset.

Similar to the CESM2 Pacific pacemaker ensemble, we utilized a 10-member ensemble of CESM1 simulations where observations (ERSSTv3b) were used to nudge time-evolving SST anomalies in the North Atlantic (5-55°N, with a linearly tapering buffer zone extending to the equator and 60°N, covering the Atlantic basin). This Atlantic pacemaker ensemble runs from 1920 to 2013, but only data for the 1950-2013 period are used. The ensemble includes all CMIP5 time-varying external, natural, and anthropogenic forcings (Yang et al., 2020). ~~The complete description and documentation of the Pacific pacemaker dataset are available on the Climate Variability and Change Working Group's (CVCWG) webpage (https://www.cesm.ucar.edu/working-groups/clima DOI: 10.26024/gtrs-tf57, last access: 01.04.2023).~~

2.3 Pre-industrial control run

To further examine the interactions between the Atlantic and Pacific modes of internal variability under unforced scenarios, we use ~~120 years (from the beginning of year 1000 to the end of 1119) of from~~ 250 years from the CESM2 pre-industrial control ~~run~~ run (representative of the period prior to 1850, Eyring et al., 2016) to extract monthly averages for the same variables as in the pacemaker simulations and reanalysis (TS, SLP, U). We use the CESM2 model for its remarkable simulation of ENSO characteristics (Danabasoglu et al., 2020; **?**; Capotondi et al., 2020; Chen et al., 2021) and also to facilitate the comparison with the pacemaker ensemble results.

2.4 Indices

We calculate the indices for TNA, Niño3.4, PNA, NAO, and the PWC with respect to 1950-2014 climatology as follows:

- TNA (Tropical North Atlantic) Index is the area-weighted monthly SSTAs over the North Tropical Atlantic region 5.5–23.5°N, 58~~W~~°–15°W (Enfield et al., 1999).
- Niño3.4 Index is the area-weighted monthly SSTAs over the equatorial pacific region 5°N–5°S, 170~~W~~°–120°W (Trenberth, 1997).
- PNA (Pacific North American) Index is the leading EOF of (~~seasonally~~ 3-monthly averaged and area-weighted) SLP anomalies over the Pacific North America region 20–85°N, 120°E–120°W (Wallace and Gutzler, 1981).
- NAO (North Atlantic Oscillation) Index is the leading EOF of (~~seasonally~~ 3-monthly averaged and area-weighted) SLP anomalies over the North Atlantic region 20-80°N, 90°W-40°E (Hurrell and Deser, 2009).
- PWC_u (Pacific Walker Circulation u component) as an index for the PWC and is defined as the monthly zonal wind anomaly at 925 hPa (or nearest available level for pacemaker simulations) over the equatorial pacific region (6°N–6°S, 180°-150°E, following Chung et al., 2019), where negative (positive) values indicate anomalous easterly (westerly) winds that imply a strengthening (weakening) of the PWC.
- ATL3 (equatorial Atlantic) Index is the area-weighted monthly SSTAs over the equatorial Atlantic region 3°N–3°S, 20°W–0° (Zebiak, 1993).

We also use indices for AMV and PDV to illustrate the decadal imprint of internal variability over the Atlantic and Pacific~~during the pre-industrial run~~, a proxy for the long-term physical state of the two basins. ~~Here~~ For the causal analysis of the pre-industrial control run, the low-pass filtered versions of these indices are used to filter out composites of the timeseries depending on the different in-phase and out-of-phase combinations of AMV and PDV. Here, the AMV and PDV indices are calculated as follows:

- AMV (Atlantic Multidecadal Variability) Index (sometimes referred to as the AMO (Atlantic Multidecadal Oscillation) index) is defined as monthly SSTAs averaged over the North Atlantic region ~~(~~0–60°N, 80–0~~W) minus the global mean (70 N–60 S, effectively detrending the data, see Trenberth and Shea, 2006)~~°W (Trenberth and Shea, 2006).
- PDV (Pacific Decadal Variability) Index (sometimes referred to as the PDO (Pacific Decadal Variability) index) is defined as the standardized principal component (PC) time series associated with the leading EOF of area-weighted monthly SSTAs over the North Pacific region ~~(~~20–70°N, 110°E–100~~W) minus the global mean (70 N–60 S, effectively detrending the data, see~~ °W (Mantua et al., 1997).

3 Methodology

3.1 Separating internal variability from the externally forced components

To isolate internal variability from the Pacific pacemaker simulations, we first calculate a multi-ensemble mean (MEM) for each variable, representing an estimate of the externally forced component. This is done by averaging three CMIP6 historical large ensemble means (with different numbers of ensemble members): CESM2 (11 members), MIROC6 (50 members), and UKESM1-0-LL (16 members). These models were chosen to represent the MEM, since they realistically simulate the spatiotemporal characteristics of the major modes of climate variability (notably ENSO and North Atlantic SST modes) during the historical period (Phillips et al., 2020; Fasullo et al., 2020; Karmouche et al., 2023). Moreover, to detect changes in various climate phenomena, the required number of members in an ensemble simulation may differ. Forced changes in ocean heat content can be detected with only a few members, while changes in atmospheric circulation or extreme precipitation and temperature may need 20-30 members (Deser et al., 2010; Tebaldi et al., 2021; Smith et al., 2022). Detecting forced changes in the characteristics of internal variability, such as its amplitude, spatial pattern, and remote teleconnections, may require even larger ensembles (Milinski et al., 2020; Smith et al., 2022; O'Brien and Deser, 2023; Deser and Phillips, 2023). The idea behind estimating the forced response from three different large ensembles with different numbers of realizations is to reduce any biases originating from the model's own representation of CMIP6 forcing and/or from the ensemble size. Because each of the 10 members in the pacemaker ensemble is subjected to the same CMIP6 time-varying external forcing, we assume that MEM is the response to external forcing such as GHG-induced warming trends, solar radiation, volcanic activity, land use changes, and anthropogenic aerosols. Consequently, the discrepancies in each pacemaker simulation relative to MEM can be attributed to internal variability. Therefore, for a given variable X ($X = SST, U, SLP$), we can express the separation in a pacemaker simulation i as:

$$X_i = X_{\text{MEM}} + X_{\text{internal}(i)}, \qquad i = 1, 2, \ldots, 10 \tag{1}$$

where X_{MEM} is the forced component estimated from the CMIP6 MEM and $X_{\text{internal}(i)}$ is the residual of the original X_i minus the forced response X_{MEM}, which varies among different members and shows the component associated with isolated internal variability. This is similar to methods from Wu et al. (2021), but using the CMIP6 MEM instead of the pacemaker ensemble mean to quantify the forced component. It should be noted that the differences between the pacemaker simulations and MEM can emerge from: i) MEM estimating a climate sensitivity (in response to external forcing) different from the one prescribed in the restoring region. ii) Outside the restoring region, the climate sensitivity of the CESM models can also be different from the one estimated by MEM there. iii) Differences can also arise from a mix of (i) and (ii).

To isolate the internal variability in observations and the pacemaker simulations following Eq. (1), we subtract the MEM for SST, SLP, and U from observations and each pacemaker simulation before calculating the indices above. Figure 1 illustrates the standardized seasonally averaged time series of Niño3.4 (a), TNA (b), PNA (c), NAO (d), ~~and~~ PWC$_u$ (e), and ATL3 (f) indices from observations for the 1950-2014 period. For each index, the time series in black represents the original indices from HadISST (a,b,f) and NCEP-NCAR-R1 (c-e), as mixed signals including external forcing (non-linear trends). The time series

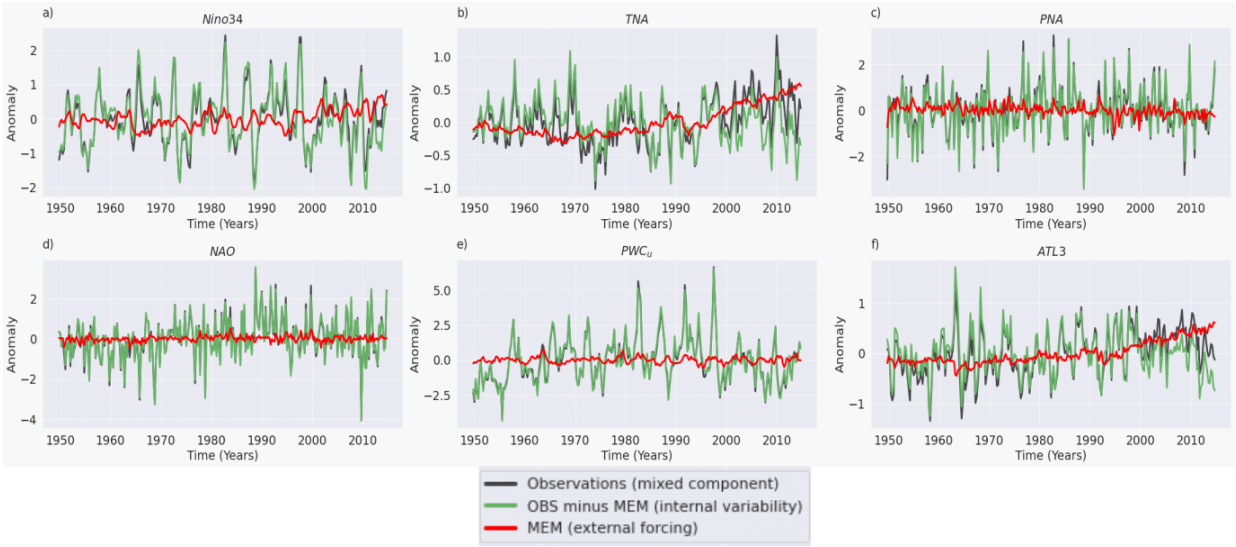

Figure 1. ~~Standardized seasonally averaged time series of a) Niño3.4, b) TNA, c) PNA, d) NAO, and e) PWC$_u$ during the observed 1950-2014 period. Unit for the standard deviations are °C in a and b, Pa in c and d, and m.s^{-1} in e. The time series in black represent the mixed signal from indices calculated using HadISST (a,b) and NCEP-NCAR Reanalysis-1 (c-e). The time series in green are calculated after subtracting the CMIP6 external forcing represented by MEM following Eq. 1 (see Sect. 3.1). In each panel, the red line denotes the difference between the black and green line at each time step, representing the varying effect of subtracting MEM on each index.~~ **Standardized seasonally averaged time series of a) Niño3.4, b) TNA, c) PNA, d) NAO, e) PWC$_u$, and f) ATL3 during the observed 1950-2014 period. Unit for the standard deviations are [°C] in a, b and f, [Pa] in c and d, and [m.s^{-1}] in e. The time series in black represent the mixed signal from indices calculated using HadISST (a,b,f) and NCEP-NCAR Reanalysis-1 (c-e). The time series in green are calculated after subtracting the CMIP6 external forcing represented by MEM following Eq. 1 (see Sect. 3.1). In each panel, the red line denotes the difference between the black and green line at each time step, representing the varying effect of subtracting MEM on each index.**

in green show the indices after subtracting MEM (producing an estimate of isolated internal variability). The difference that denotes the effects of external forcing is shown in red. Based on Fig. 1, ~~there are two indices that~~ three indices expose positive trends represented by ~~external forcings~~increased external forcing during the second half of the analyzed period, namely Niño3.4 (a) and more clearly TNA (b) and ATL3 (f). The rest of the analyzed indices do not show distinctive trends nor significant effects of external forcing.

3.2 PCMCI+ algorithm for causal discovery

Similar to methods from Karmouche et al. (2023), we use the PCMCI+ causal discovery algorithm, part of the freely available Tigramite python package (https://github.com/jakobrunge/tigramite, last access: 03.07.2023) to efficiently estimate causal networks from time series datasets (Runge et al., 2019), and detect lagged (τ>0) and contemporaneous (τ=0) causal links (Runge,

2020), where τ stands for the time lag. The full description of the method and pseudo code, along with explanations of the underlying assumptions for causal interpretation, can be found in Runge et al. (2023) and Runge (2020), respectively. Crucially, to interpret obtained links in PCMCI+ as causally directed, the method assumes that no unobserved confounders exist.

The PCMCI+ algorithm consists of two main phases: skeleton discovery and orientation. The skeleton discovery phase starts with the PC1 Markov set discovery algorithm, which is based on the PC algorithm (Peter Spirtes and Clark Glymour), to test for conditional independence of pairs of variables, and it is followed by a momentary conditional independence (MCI) test to remove spurious links due to contemporaneous confounders (Runge, 2020). The orientation phase orients contemporaneous links based on unshielded triples, and the resulting graph contains directed lagged and contemporaneous links as well as unoriented contemporaneous adjacencies (Markov equivalence) or conflicting adjacencies (see rules R1–R3 in Runge, 2020). ~~The resulting links are then visualized as a process graph that summarizes causal dependencies and their time lags. Here, we estimate the link strengths as standardized (causal)regression coefficients (Runge et al., 2015) using a linear mediation model from the actual parents estimated by~~ We primarily apply partial correlation *ParCorr* as an independence test for the analysis, except in the proof of concept (Section 3.2.1) where we opt for *RobustParcorr*. *ParCorr* assesses partial correlation by regressing out the effect of a conditioning variable through linear ordinary least squares regression. While *RobustParcorr* is similar, it first transforms variables to the standard normal marginals which is particularly useful when dealing with non-gaussian distributed variables (which is the case for variables in Sect. 3.2.1; see skewed data in density plots in the Supplementary Fig. S1).

There are two main free parameters for PCMCI+. First, the maximum time lag τ_{max}, which is decided after analyzing the lagged dependencies between the variables (see lag function plot in Supplementary Fig. S2) and literature review. The second parameter is α_{pc}, which represents the significance threshold adopted for all PCMCI+ tests. The algorithm outputs a *p-matrix* (containing the *p-values*, denoting the uncertainty of each link) and a *val_matrix* (containing the *cross-MCI*, translating the strength of each link). The *p-values* for the coefficients shown on a PCMCI+ ~~. More precisely, we estimate each variable X_t^j on its parents $pa(X_t^j)$. Then, the regression coefficients corresponding to each parent provide a link coefficient with a causal interpretation under the above assumptions. Considering X and Y are variables represented by their time series~~ causal graph are below the significance threshold α_{pc}. We note that these are valid only for the adjacencies and not the directionality of contemporaneous links decided during the orientation phase (lagged links are always oriented according to time order). The limitation presented by the absence of comprehensive confidence measures for all PCMCI+ estimated links is an aspect currently being addressed where bootstrap aggregation methods are still under review (Debeire et al., 2023, in review). In the context of this paper, the *p-value* matrices are shown in Supplementary material (e.g. Figs. S3, S6, S8) to provide a measure of the uncertainties of the estimated adjacencies. The Tigramite package offers the ability to plot results in the form of a causal graph where nodes represent the time series associated with each variable. In these graphs, the node color shows the auto-MCI value (auto-correlation i.e. self links) and the link color indicates the cross-MCI value (i.e. link strength) with blue indicating opposite-sign (negative) inter-dependency and red indicating same-sign (positive) inter-dependency. The link-associated time lags are shown as small labels on the curved links. If a link is detected at different lags, the indicated lags are sorted by link strength (i.e. by the absolute cross-MCI value). Contemporaneous links (at lag zero) are represented by straight lines. In the context of causal links between variables X_i and X_j at time t, the possible link types considered for any time lag (τ) are

non-adjacent links (i.e., the pair is not directly connected) and direct links from X_i at time $t-\tau$ to X_j at time t ($X_i^{t-\tau} \to X_j^t$). For $\tau = 0$ additional possible link types are opposite direct links ($X_i^t \leftarrow X_j^t$), unoriented links ($X_i^t \circ\!\!-\!\!\circ X_j^t$), and conflicting links ($X_i^t \times\!\!-\!\!\times X_j^t$) which can occur due to finite sample effects or violations of assumptions. While we tolerate the presence of unoriented adjacencies due to Markov equivalence ($X_i^t \circ\!\!-\!\!\circ X_j^t$, hereafter denoted by "o-o" symbol) in the causal graphs of the upcoming sections, we introduce assumptions for the cases where conflicting links ($X_i^t \times\!\!-\!\!\times X_j^t$) occur. For the analysis of the Pacific and Atlantic pacemaker ensembles (Sect 4.2), we introduce these assumptions on the basis of which variables have been nudged toward observed values. For example, in the ~~time lag τ, if we assume causal sufficiency and that the linear model is suitable, then the link coefficient (link coeff.) of $X_{t-\tau}$~~ PCMCI+ tests on the pacific pacemaker simulations, the implemented assumption states that if the method detects a contemporaneous adjacency between Niño3.4 and any other variable X, then the link should be directed from Niño3.4 to ~~Y_t obtained from standardized time series tells us how much the expected value of Y_t (measured in standard deviation units) will change if $X_{t-\tau}$ is changed by one standard deviation. Note that the PCMCI~~X ($Niño3.4 \to X$). This is because Niño3.4 is the pacemaker as the SSTA is nudged towards observations in that region. We follow the same approach for the Atlantic pacemaker, where the assumptions presume only outgoing contemporaneous links from TNA (as the SSTAs in that region are nudged to observations). Additionally, some other assumptions are introduced to not estimate specific links (having no physical basis according to well-established literature) or to overcome specific cases of "$\times\!\!-\!\!\times$"-type links by presuming their orientation according to background knowledge (well-defined physics from previous studies) and/or sensitivity tests (using different conditional independence tests, different α_{pc} and/or sliding window analysis). While no assumption is predefined in next section's proof of concept, the assumptions introduced in each of the Results subsections (Sects. 4.1-4.3) are explained in detail at the end of Sect. 3.2.2. In Supplementary material, we show all original PCMCI+ ~~resulting graphs may contain unoriented as well as conflicting links at lag zero (e.g. due to Markov equivalence and conflicting orientation rule applications) . Here we orient these links to satisfy a (fully-oriented) Directed Acyclic Graph (DAG)based on the direction in which they most appeared in all instances of that particular contemporaneous link across the CESM2 pacemaker ensemble during each regime. The set of directions learned from the majority ruling is used to direct unoriented links during the reanalysis and the pre-industrial control runs as well. Such adjustment is practiced while ensuring no occurrence of contemporaneous cycles. Table S1, part of Supplementary Material, shows the originally unoriented contemporaneous links , their instances, their new directions, andthe basis on which the directions were decided.~~ graphs that possibly contain conflicting edges ($X_i^t \times\!\!-\!\!\times X_j^t$) and where all dependencies between all variables at all lags are considered (i.e. no assumptions introduced).

3.2.1 Proof of Concept: the 1997/1998 El Niño

The ENSO phenomenon has been a subject of intense scientific interest due to its profound impacts on global climate patterns. Among the ENSO events, the El Niño of 1997/1998 stands out as one of the most powerful and influential episodes in recorded history. The processes and the feedbacks involved with this event are relatively well understood and documented (e.g. McPhaden, 1999; Lengaigne et al., 2003). Thus, as a proof of concept for our methodology, we apply causal discovery to analyze this event and to physically interpret it in the context of well-known processes. This will provide insight to point

toward the causal analysis in this paper of the less well-understood interactions between the Pacific and the Atlantic. Through the application of the PCMCI+ causal discovery algorithm, we identify potential cause-and-effect relationships among the selected variables, shedding light on the intricate interactions that contributed to the onset and intensification of the 1997/1998 El Niño event. Candidate variables for this case study, which have been used in previous studies (Trenberth, 1997; Neelin et al., 1998; McPhaden, 1999; Lengaigne et al., 2003; Wang, 2018) and thus applied here, include the SSTAs over the Niño3.4 region (SST Niño3.4), ~~precipitation over~~ eastward wind anomalies in the central Pacific (~~Precip~~ Uwind CPAC), the wind stress over the west Pacific (Wind_{Stress} WPAC), the east-west SLP anomaly gradient (SLP_{grad} EPAC-WPAC), and the depth of thermocline in the east Pacific (Tcline_{Depth} EPAC). We extract these variables as monthly averages between January 1995 and December 1999 from NCEP-NCAR-R1, HadISST, and two reanalysis datasets from the European Centre for Medium-Range Weather Forecasts (ECMWF), namely, the Ocean Reanalysis System 5 (ORAS5, Copernicus Climate Change Service, 2021) and ERA5 (Copernicus Climate Change Service, 2019) datasets. This means that the PCMCI+ data frame in this section has a length of 60 time steps (months) with 5 variables, which are listed in Table 1 with their respective details.

Table 1. Climate variables used in the 1997/1998 El Niño case study

Variables (nodes)	Dataset	Definition	Region
SST Niño3.4	HadISST	SSTAs over the Niño3.4 region [$°C$]	5°S-5°N, 170°W-120°W
~~Precip~~ Uwind CPAC	~~ERA5~~ NCEP-NCAR-R1	~~Central Pacific Precipitation Anomalies~~ Westerly Wind Anomalies in Central Pacific [$m.s^{-1}$]	5°S-5°N, ~~170~~180°~~W-120~~W-150°W
Wind_{Stress} WPAC	ORAS5	West Pacific Wind Stress Anomalies [$N.m^{-2}$]	5°S-5°N, 140°E-170°E
SLP_{grad} EPAC-WPAC	~~NCEP Reanalysis 1~~ NCEP-NCAR-R1	East-West Sea Level Pressure Anomaly Gradient [Pa]	[5°S-5°N, 100°E-160°E] minus [5°S-5°N, 100°W-160°W]
Tcline_{Depth} EPAC	ORAS5	Depth of 20°C Isotherm in the Eastern Pacific [m]	5°S-5°N, 150°W-120°W

~~The Tigramite package offers the ability to plot causal networks where nodes represent the time series associated with each climate variability index. Node colors indicate the coefficient of the self-links (auto-coefficient) for each time series, and the colors of the links (arrows) denote the linear link coefficients, with blue indicating opposite-sign (negative) inter-dependency and red indicating same-sign (positive) inter-dependency strength. The link-associated time lags are shown as small labels on the curved links. If a lagged link is detected more than once, the indicated lags are sorted by strength (sorted by the absolute value of the link coefficient). During this proof-of-concept~~ During this proof of concept section, we estimate depen-

dencies only for lags between ~~1~~ 0 and 3 months (τ_{min} = ~~1~~0, τ_{max} = 3) ~~. This is due to data availability and also because the inter-dependencies happening on a daily-to-weekly timescale are not within the scope of this paper. For this ENSO study, the~~ and set the significance threshold α_{pc} to 0.1. The parameter τ_{max} is generally decided after inspecting a lagged dependency matrix (see Supplementary Fig. S2). The PCMCI+ algorithm detected causal links between the variables (see time series in Fig. 2a) that can be summarized through the causal network shown in Fig. ~~2. We show the time series of each variable next to each node shown in the causal network.~~ 2b. The uncertainties for all coefficients in Fig. 2b can be found in the Supplementary Fig. S3.

The results obtained from the PCMCI+ algorithm confirm previous insights into the mechanisms leading to the 1997/1998 El Niño event and its intensification by identifying significant causal links among the variables. One crucial node with ~~multiple originating~~ only outgoing links is Wind$_{Stress}$ WPAC, indicating ~~its central role in driving various aspects of the~~ the central role of the March 1997 westerly wind bursts in triggering the 1997/1998 El Niño~~phenomenon.~~

~~The links from Wind$_{Stress}$ WPAC are~~ , by generating a downwelling eastward-propagating Kelvin wave, as evidenced by previous studies (Lian and Chen, 2021; Lengaigne et al., 2002, 2004). The Bjerknes feedback, which is essential in generating El Niño, is also clearly detected in the resulting causal network. This positive feedback loop involves a coupling between wind, thermocline depth, and SST where a weakening of the equatorial trade winds (westerly wind anomalies) in the West is associated with the deepening of the thermocline in the east. The westerly anomaly winds reduce the upwelling and, along with the deepened thermocline, contribute to warming SSTs in the central and east Pacific. This weakens the East-West SLP and temperature gradients, thus contributing to further weakening of the easterly winds, and so on. These processes are summarized in the causal graph as follows:

~

- Wind$_{Stress}$ WPAC → Tcline$_{Depth}$ EPAC with a 1-month lag and as same-sign response. This link indicates that the westerly wind burst in the West Pacific contributed to an increase in the thermocline depth in the Eastern Pacific during the following month (associated with an eastward propagating downwelling Kelvin wave in the ocean as previously documented). As the thermocline deepens in the east, upwelling brings up warmer water from the thickened thermocline, contributing to the warming of SSTs in the central and eastern equatorial Pacific.

- Wind$_{Stress}$ WPAC → ~~SST Niño3.4 with a 2-month lag and as same-sign response. This link indicates that as the wind stress over the West Pacific increases, it causes the SST anomalies over the Niño3.4 region to increase with a lag of 2 months. The deepening of the thermocline in the east and the reduction in the upwelling of colder waters further contribute to the anomalous warming of SSTs in the central and eastern equatorial Pacific.~~

- ~~Wind$_{Stress}$ WPAC →~~ SLP$_{grad}$ EPAC-WPAC ~~with a 3-month lagand as~~ contemporaneous (zero lag) opposite-sign response. This link indicates that the westerly wind burst in the West Pacific contributes to ~~a three-month lagged~~ the decrease in the sea-level pressure gradient between the East and West Pacific. The decreasing SLP gradient means that the sea level pressures over the West Pacific become anomalously higher than those in the East Pacific~~, contributing to changes in atmospheric circulation and the thermocline depth~~.

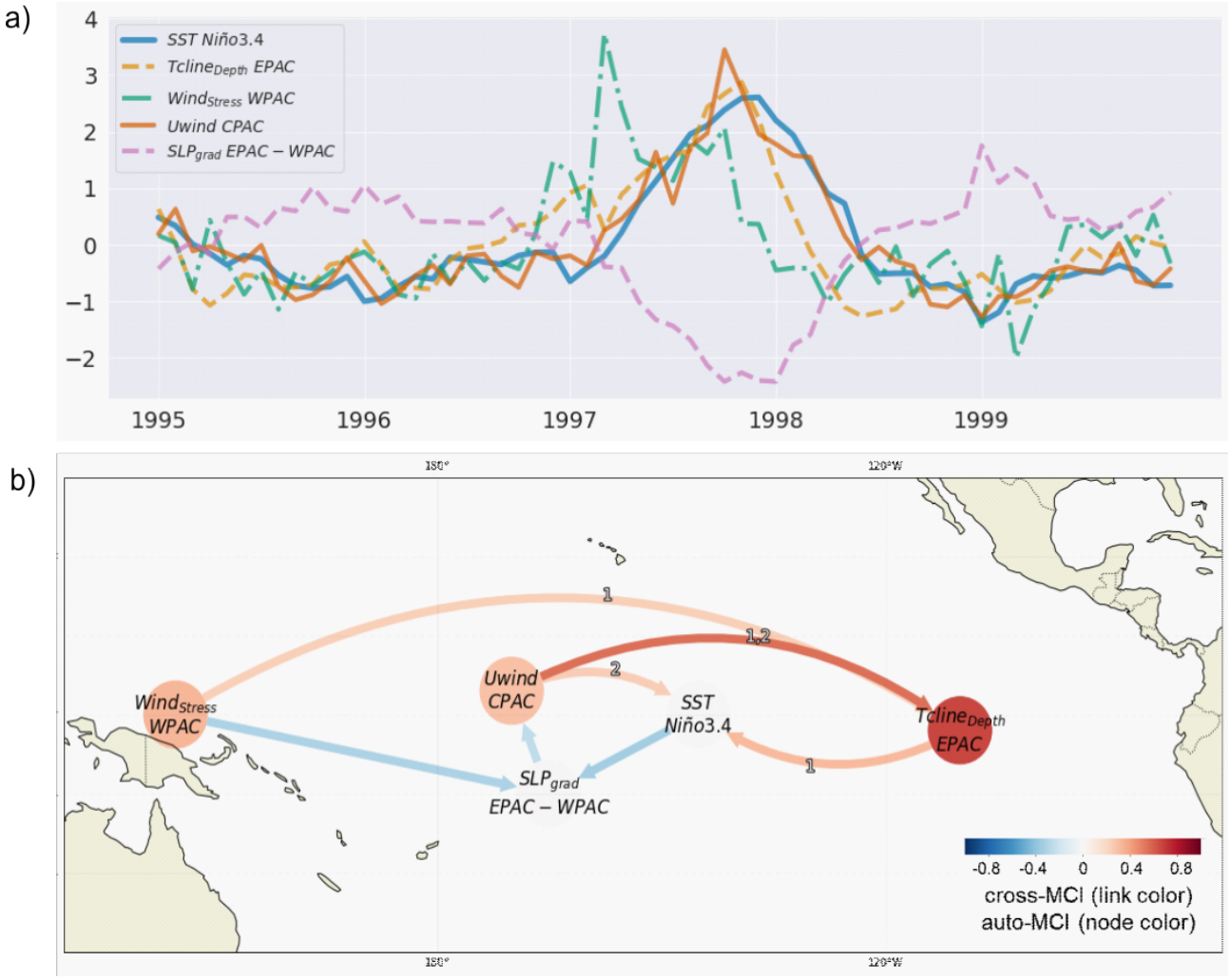

Figure 2. ~~Causal networks representing lagged causal links between the variables in Table 1 for the 1997-1998 El Niño event. Constructed by applying PCMCI+ on the detrended time series of each variable between January 1995 and December 1999. Nodes represent the time series associated with each climate variable (see node labels and details in Table 1). Node colors indicate the self-link coefficients of each time series (auto-coeff, see color bar), and the color of the links denotes the linear link coefficient (link coeff, see color bar). The link-associated time lags (unit=1 month) are shown as small labels on the links.~~ Causal analysis for the 1997-1998 El Niño event. a) Detrended standardized monthly time series of the variables listed in Table 1 between 1995-1999. b) Causal network representing lagged (curved) and contemporaneous (straight) causal links, constructed by applying PCMCI+ on the time series in (a). Nodes represent the time series associated with each climate variable (see node labels and details in Table 1). Node colors indicate the self-link strengths (autocorrelation) of each time series (auto-MCI, see color bar), and the color of the links denotes the cross-link strengths (cross-MCI, see color bar). The link-associated time lags (unit=1 month) are shown as small labels on the links.

- ~~Wind$_{Stress}$ WPAC~~ Tcline$_{Depth}$ EPAC → ~~Precip CPAC with a 3-month~~ SST Niño3.4 with a 1-month lag and as same-sign response. ~~The~~ This link indicates that as the depth of the thermocline in the ~~anomalous increase in wind stress in the West Pacific contributes to an increase in Central Pacific precipitation after three months of the wind burst. Although no link originating from Precip CPAC was detected, the shift in precipitation patterns further amplifies the anomalous warming in the~~ East Pacific increases, it contributes to the SST anomalies over the Niño3.4 region ~~due to reduced upwelling and the Bjerknes feedback.~~

~~The links from SST Niño3.4 are as follows:~~

- ~~SST Niño3.4 → Precip CPAC with a 1-month lag and as same-sign response. This link means that the rising temperatures in the Central Pacific Niño3.4 region contributed to the increased rainfall over the same region after a one-month lag. The changes in precipitation patterns further affect the atmospheric and oceanic conditions, reinforcing the warming in the Niño3.4 region~~to increase with a lag of 1 month. This is due to the reduction in the upwelling of colder waters, further contributing to the anomalous warming of SSTs in the central and eastern equatorial Pacific, which represents one of the three components of the Bjerknes feedback.

- SST Niño3.4 → SLP$_{grad}$ EPAC-WPAC ~~with a 1-month lag and as~~ → Uwind CPAC as contemporaneous opposite-sign ~~strong response. This link suggests~~ responses. These links indicate that the rising temperatures over the Niño3.4 region ~~greatly decrease~~ are associated with the decrease in the East-West ~~sea-level pressure~~ SLP gradient. This reduction in the SLP gradient contributes ~~as an indicator of a~~ to the anomalous westerlies and the weakening of the Pacific Walker ~~Circulation, further impacting atmospheric and oceanic conditions during the El Niño event.~~

~~The link from~~ circulation as shown by the negative SLP$_{grad}$ EPAC-WPAC ~~is as follows:~~

- ~~SLP~~ → Uwind CPAC link. This constitutes the second component of the Bjerknes feedback. As mentioned earlier, the westerly wind burst also contributes to the below-normal SLP gradient at lag zero (Wind$_{Stress}$ WPAC → SLP$_{grad}$ EPAC-WPAC).

- Uwind CPAC → Tcline$_{Depth}$ EPAC with a ~~3-month~~ 1-month lag and a strong same-sign response. This link ~~suggests that the decreasing East Pacific SLP anomalies (compared to the West Pacific), associated with both rising SSTs in the Niño3.4 region and the preceding increased Wind Stress over the West Pacific, contribute to a decrease in the thermocline depth over the East Pacific. However~~shows that the westerly wind anomalies weaken the PWC and strongly contribute to the deepening of the thermocline. While Wind$_{Stress}$ WPAC → Tcline$_{Depth}$ EPAC is essential to trigger the 1997/1998 El Niño event, this link ~~'s interpretation is tricky, as it suggests that the SLP gradient decreasing would cause the thermocline to become shallower after three months, which is opposite to the one-month lagged strong increase due to the West Pacific wind burst. This link color, on the other hand, suggests that the effect of WindStress WPAC~~ is necessary to maintain a strong El Niño state and corresponds to the third component of the Bjerknes feedback, hence, closing the loop. A Uwind CPAC → Tcline$_{Depth}$ EPAC ~~is stronger in driving changes in the thermocline depth during the El Niño event than the 3-month lagged SLP$_{grad}$ EPAC-WPAC~~ link is also found at a 2-month lag with a lower absolute cross-MCI value.

– Uwind CPAC → SST Niño3.4 with a 2-month lag and a same-sign response. This lagged link represents the same effect of the Uwind CPAC → Tcline$_{Depth}$ EPAC ~~link.~~ → SST Niño3.4 connection at 2-month lag.

To summarize, a causal analysis has been applied to the El Niño event of 1997/1998 to demonstrate the utility of such an analysis in quantifying the connections between physical processes. Previous results are confirmed by this causal analysis in that the westerly wind burst event in the western equatorial Pacific in March triggered an eastward traveling downwelling Kelvin wave in the ocean that deepened the thermocline in the east and shallowed it in the west. As SSTs warmed in the eastern equatorial Pacific, trade winds weakened. This weakening further reduced the upwelling of cold, nutrient-rich waters in the eastern Pacific and instead brought up relatively warmer water from the thickened thermocline, contributing to the warming of SST in the Niño 3.4 region. The identified causal links align with the mechanisms involving the Wind$_{Stress}$ WPAC influencing thermocline depth, ~~and leading~~ which then leads to anomalous warming in the Niño3.4 region, in agreement with extensive previous studies ~~(McPhaden, 1999; Lengaigne et al., 2003)~~(McPhaden, 1999; Lengaigne et al., 2002, 2003, 2004). Furthermore, the Bjerknes positive feedback is well demonstrated through the weakening of easterly winds, causing a deepening of the thermocline in the east, which consequently warms Niño 3.4 SSTs. The anomalously warm SSTs contribute back to the weakening of easterly winds through adjustment of the East-West SLP ~~anomalies and~~ gradient and ultimately closing the loop. Although not included in this analysis, anomalous shifts in precipitation patterns are ~~shown to be~~ also greatly affected by the SST variations ~~in the central east Pacific as hypothesized, and this further contributes~~ and further contribute to the intensification and maintenance of the 1997/1998 El Niño event.

The advantage of applying causal discovery is that many hypothesized interactions are analyzed simultaneously within one single data frame and multiple connections are estimated while controlling for spurious associations. This represents an advantage over conventional paired regressions, correlations, or multiple regression techniques which cannot always reveal the underlying cause-and-effect relationships among variables.

With this demonstration of the utility of causal analysis in quantifying connections between phenomena that represent previously documented physical processes, we now apply the causal methodology to the less well-understood problem of the nature of the connections between the Pacific and Atlantic.

3.2.2 PCMCI+ application to Atlantic-Pacific connections

On the time resolution of the PCMCI+ data frames used in Sect. 4, we note that we use ~~seasonally~~ 3-monthly averaged time series of each index (TNA, ATL3, Niño3.4, PNA, NAO, and the PWC$_u$) with four seasons (time steps) per year, as averages of ~~January-February-March (JFM), April-May-June (AMJ), July-August-September (JAS), and October-November-December (OND~~DJF (December, January and February), MAM (March, April and May), JJA (June, July and August) and SON (September, October and November). For the parameter settings of the PCMCI+ algorithm, we set the maximum time lag to ~~8~~ 4 time steps (τ_{max} = ~~8~~ 4 [seasons]), meaning that we only investigate teleconnections within a maximum of ~~two-year~~ one-year time lag. Additionally, we ~~also look at~~ estimate contemporaneous links detected within the same season (τ_{min} = 0). ~~These contemporaneous inter-dependencies that happen with no time lag (i.e., τ<1) are shown as straight links on the causal networks (Sect. 4).~~ The

significance level ~~of the MCI partial correlation tests α_{pc}~~ α_{pc} of all tests carried during the PCMCI+ algorithm in Sect. 4.1 is set to 0.2 to account for the short sample ~~size.~~ sizes. As more data is available for the pacemaker ensembles (10 simulations each, Sect. 4.2) and the pre-industrial control run (Sect. 4.3), α_{pc} is set to 0.01 and 0.05, respectively. It is important to note that the networks are only causal with respect to the analyzed variables, and more advanced methods that can deal with hidden variables (Gerhardus and Runge, 2020) may not be suitable for short sample sizes.

4 ~~Results~~

3.1 ~~Observed teleconnections in Reanalysis datasets~~

3.0.1 ~~Correlation and regression patterns~~

~~To demonstrate the relationships between Atlantic and Pacific SST modes and to estimate the effect of removing the externally forced signal (represented by MEM, for more details see Sect. 3.1) from~~ As we employ multiple simulations corresponding to the ~~original SSTs, we first calculate Pearson's correlation between global SSTAs with SST-derived indices based on the original HadISST dataset.~~ **~~Regression pattern of global SST anomalies (SSTAs) onto Niño3.4 index (a,c) and TNA index (b,d) during both periods: 1950-1983 (top) vs 1985-2014 (bottom). a) Pearson's correlation coefficients (shadings) and regression coefficients (contours) of detrended global SSTAs with the standardized Niño3.4 index based on HadISST data during 1950-1983. b) Same as (a) but showing the SSTAs correlation and regression with the standardized TNA index instead of Niño3.4. c) Same as (a) but for the 1985-2014 period. d) Same as (b) but for the 1985-2014 period. White-shaded areas indicate weak correlations (between -0.1 and 0.1). The contour interval is 0.2 (°C) with dashed (solid) contours indicating regions with negative (positive) regression coefficients. Global SSTAs are detrended by removing the global mean at each time step. For convenience, the dashed black box shows the considered TNA region.~~**

~~Similar to Fig. 3 but after removing the externally forced signal represented by MEM following Eq. (1) (see methods Sect 3.1.). All SST fields have the CMIP6 MEM subtracted prior to calculating anomalies and performing the regressions.~~

~~Figure 3 displays the regression patterns of global SSTAs during two distinct regimes: the Pacific-driven 1950-1983 period (Fig. 3a and b) and the Atlantic-driven 1985-2014 period (Fig. 3c and d). The analysis~~ same ensemble during the causal analysis of pacemaker time series in Sect 4.2, we utilize the Multidata-PCMCI+ function that allows testing for conditional independencies by combining samples taken from several datasets (i.e. other simulations in the pacemaker ensemble) and learning a single causal graph representing the shared underlying processes. Concerning Sect. 4.3, we show results based on composites selected depending on the phase combination of PDV and AMV (i.e. PDV+/AMV+, PDV-/AMV+, PDV+/AMV- and PDV-/AMV-). A mask is used on the PCMCI+ data frame to select only time steps that satisfy a certain combination. A similar "regime-oriented" analysis is detailed in Fig. 3 ~~focuses on the relationship between SSTAs and two key climate indices (namely Niño3.4 and TNA indices) using the original SST signal, hypothesized to contain influences of both internal variability and external forcing (as discussed~~ of Karmouche et al. (2023). Here, we only use this approach for the pre-industrial control

run because larger sample sizes are available and such sampling at lower intervals on the short reanalysis and pacemaker data might produce "spurious" results (Smirnov and Bezruchko, 2012).

Throughout the analysis in Sect. ~~3.1 and seen in Fig. 1a and b). Figure~~ 4, ~~on the other hand, shows the same analysis but after isolating the internal variability component of the SST modes and anomalies by subtracting MEM from the original SST fields following Eq.~~ the results are shown for PCMCI+ runs where assumptions have been introduced. Next, we list and discuss all assumptions that were introduced into the analysis. First, to focus on the Atlantic-Pacific interactions, we do not estimate any contemporaneous or lagged dependencies between (1) ~~. For both Fig. 3 and 4, the top panel (a) illustrates Pearson's correlation coefficients and regression coefficients between detrended global SSTAs and the standardized~~ TNA and ATL3, (2) ATL3 and NAO, (3) ATL3 and PNA, and (4) PNA and PWC_u. Although the AZM (ATL3) can be associated with changes in AMM (comprising TNA) through the meridional displacements of the ITCZ, the two modes remain independent and are not considered to affect one another directly (assumption 1, Masson-Delmotte et al., 2023; Murtugudde et al., 2001). The same is true for a direct ATL3-NAO relationship, which was found to be weak and not statistically significant in previous studies (e.g. Wang, 2002, assumption 2). A direct link between PNA and ATL3 is disregarded because there is no proposed physical mechanism for such connection without a major role of ENSO and PWC and also because the main link connecting tropical Atlantic and extratropical Pacific happens through TNA SSTAs' relationship to the pressure system over southeastern United States (assumption 3, Klein et al., 1999; García-Serrano et al., 2017b; Jiang and Li, 2019). Moreover, we consider the PWC to only be connected to PNA through ENSO (e.g. via a poleward-propagating Rossby wave in the case of an El Niño event, Wallace and Gutz , hence, we estimate the ENSO-PNA connection only through the Niño3.4~~index for the period 1950-1983, based on HadISST data. Similarly, the second panel (b) presents the same correlation and regression analysis but with the standardized TNA index instead of~~ -PNA pair (assumption 4). Assumptions 1-4 are held throughout all results shown in Sect. 4. Additionally, during the PCMCI+ analysis of the Pacific pacemaker ensemble (Sect. 4.2.1) we assume that 5) if a contemporaneous connection is estimated between Niño3.4 and any other node, then the link should be oriented from the Niño3.4 ~~. The bottom panels (c) and (d) replicate the analyses from panels (a) and (b) but for the period 1985-2014. To visualize the impact of subtracting MEM, the reader can compare one panel from Fig. 4 to its respective panel in Fig. 3.~~

~~**SSTAs regression onto the Niño3.4 index.**Before removing external forcing, during the 1950–1983 period (Fig. 3a), we find weak correlations between~~ node toward the other variable node (assumption 5) because the SSTA is nudged to observed values in the Niño3.4 ~~index and SSTAs over most of the Atlantic with negative values extending from the European west coast and decaying north of the TNA region (black dashed box in Fig. 3a). Within this TNA region, there are weak positive correlations extending from the Gulf of Mexico and decaying around the center of the TNA region. This positive relationship is consistent with several previous studies (Enfield and Mayer, 1997; Klein et al., 1999; García-Serrano et al., 2017b; Jiang and Li, 2019) that suggest warm (cold)SSTAs develop over the TNA region and peak during the spring and summer following an El Niño (La Niña) winter (Park et al., 2023b). These positive values vanish when analyzing the 1985-2014 period (Fig. 3c) , where the TNA region shows mainly values between -0.1 and 0.1 for the~~ region. Additionally, to avoid lagged links from PWC_u to Niño3.4 ~~index correlation with the SSTAs over that region (see the black dashed box in Fig. 3c). In the North Pacific, both periods show positive correlations extending along the west coast of North America, and negative correlations in the~~

central North Pacific. This horseshoe-like pattern is consistent throughout all SSTA-Niño3due to their strong relationship, we do not estimate the influences on Niño3.4 regression maps (panels a and c in Fig. 3 and Fig. 4). Comparing Fig. 4a to Fig. 3a, we conclude that although the positive correlations of tropical Atlantic SSTAs with the from past PWC$_u$ (no PWC$_u$ →Niño3.4 index slightly increased when subtracting MEM during the Pacific-driven 1950-1983 period, the impact of removing the externally forced signal is not pronounced. This conclusion also holds for the SSTA-Niño3.4 correlations during the 1985-2014 regime as there are no major differences between the TNA box (dashed box) in Fig. 4c compared to the one in Fig. 3c. **SSTAs regression onto the TNA index.** During the first period (1950-1983), the results suggest no major difference in the relationship between the TNA index and North Pacific SSTAs before and after removing external forcing. The correlation maps for the Pacific-driven regime (Fig. 3b link at any lag) in Sect. 4.2.1. Similarly, specific to the PCMCI+ analysis of the Atlantic pacemaker ensemble (Sect. 4.2.2), we assume that 6) if a contemporaneous connection is estimated between an Atlantic SST index (TNA, ATL3) and any other variable, then the link should be oriented from the Atlantic node toward the other node and the same for the direction of the contemporaneous NAO-PNA connection which is assumed as NAO → PNA (as this was the most estimated direction when no assumption is introduced, see Supplementary Fig. S13). This is because SSTA over the TNA region is nudged toward observations, and a part of the ATL3 region is included in the linearly tapering buffer zone that extends to the equator (assumption 6). The ensemble-averaged time series (with 25th-75th percentile range shading) for all indices calculated from the Pacific and 4b) show mainly positive values in the central equatorial Pacific and negative values in the central North and central South Pacific, similar to the symmetric horseshoe pattern observed from the Atlantic pacemaker simulations are shown in Supplementary material Figs. S4 and S5, respectively. On another note, 7) the contemporaneous link between Niño3.4 regressions shown in Fig. 3a and 4a. Conversely, the subsequent 1985-2014 Atlantic-driven period, where externally forced warming projects greatly onto the Atlantic SST changes (Mann et al., 2014; Klavans et al., 2021, 2022), Fig. 3d shows negative correlation values of TNA index with SSTAs over the eastern Tropical and North Pacific. However, and PWC$_u$ was detected as a conflicting link in several instances when no assumption is introduced (see odd-numbered Figs. S7-15 in Supplementary material). This might be due to the positive Bjerknes feedback loop inadequately captured on the 3-monthly averaged time resolution. Consequently, we assume this connection to be directed as PWC$_u$ → Niño3.4 (assumption 7) as this direction occurred the most frequently in the removal of the external forcing resulted in a strengthened dipole SSTA pattern over the North Atlantic and weak positive correlations over the central and eastern equatorial Pacific (Fig. 4d). The removal of external forcing suppressed the negative relationship between the TNA index and SSTAs over the tropical and northeastern Pacific during the 1985-2014 period (Fig. 4d)analysis of reanalysis data without any assumptions (excluding unoriented and conflicting links). Assumption 7 is not valid for the PCMCI+ analysis on the Pacific pacemaker ensemble (Sect. 4.2.1), where assumption 5 holds. Finally, to overcome specific instances of conflicting links in Sect. 4.1 between Niño3.4 and ATL3 (analysis of the observed historical period), we 8) assume the orientation of the same-sign contemporaneous Niño3.4-ATL3 connection as Niño3.4 → ATL3 (assumption 8). It is also important to highlight that the impact of external forcing is much more pronounced during 1985-2014, given the clear differences in the Pacific sector between the correlation maps in Fig. 3d and 4d, and which falls in agreement with previous studies (Meehl et al., 2013; Dong et al., 2014; Kucharski et al., 2015; Dong and McPhaden, 2017; Meehl et al., 2020). This suggests

~~that external forcing might have played a major role in the recent effect of the Atlantic on the Pacific.~~ However, ~~the nature of these connections remains unclear. Next, the causal discovery methodology will be applied to better quantify these connections to provide insights into the relevant physical processes.~~

3.0.1 ~~Causal networks~~

it should be noted that the relationship set by assumption 8 is fragile as discussed in Chang et al. (2006) and the same-sign effect proposed by Latif and Grötzner (2000) for ENSO's influence on Atlantic Niños was found to lag by 6 months. All causal graphs obtained without introducing any assumption are shown in odd-numbered supplementary material Figs. S7-15.

4 Results

4.1 Observed teleconnections in Reanalysis datasets

To investigate the ~~teleconnections during the two periods~~ changing interactions and the effect of external forcing during the second half of the 20th and early 21st century from a causal discovery perspective, Fig. ~~5~~ 3 demonstrates causal networks of Atlantic-Pacific teleconnections based on indices ~~from~~ listed in Sect. 2.4 from the Reanalyses datasets (Sect. 2.1). ~~The left panels in Fig. 5 (a,c) show the resulting causal networks during the 1950-1983 Pacific-driven period, while the panels on the right (b, d) show the networks for the 1985-2014 Atlantic-driven period. For each period, the panel on top (a, b) represents~~ We first show the long-term state of the Pacific and Atlantic basins represented by the 10-year low-pass filtered PDV and AMV in Fig 3a. Figure 3b shows a sliding window analysis using PCMCI+ where five periods are analyzed (1950-1970, 1960-1980, 1970-1990, 1980-2000, and 1990-2010) using the original observed signal (corresponding to the black curve in Fig. 1). ~~The bottom panel shows the networks~~ Figure 3c is similar but showing results where indices have been calculated after subtracting ~~the MEM, effectively isolating~~ MEM, estimating an isolated internal variability (corresponding to the green curve in Fig. 1). ~~In the bottom panels (c) and (d) the MEM is subtracted from the reanalyses before PCMCI+ is applied.~~ Picturing Niño3.4, PNA and PWC$_u$ as variables representing the Pacific~~while TNAand NAO represent~~ , with TNA, ATL3, and NAO representing the Atlantic, we can, for example, ~~look at~~ estimate how nodes from the Pacific basin are linked to ~~each other and to~~ the Atlantic ones, and vice-versa.

As a general note, based on Fig. ~~5~~ 3 (all panels), we detect the extensively studied relationship of ENSO and PWC (**???**), illustrated through the strong ~~positive~~ same-sign contemporaneous causal connection from PWC$_u$ to the Niño3.4 (~~(~~PWC$_u$ $\rightarrow_u$ $\rightarrow$Niño3.4 link). We confirm that positive ~~values of~~ PWC$_u$ values indicate anomalously weak easterly winds associated with the weakening of PWC and the emergence of El Niño events. With PWC inextricably linked to Niño3.4, a conclusion solidified throughout the results in Sect. 4.2 and 4.3, we consider causal links to and from a PWC$_u$ node to denote a causal relationship associated with ENSO ~~.~~ (considering the assumptions listed in Sect. 3.2.2). We also find a weak ~~opposite sign~~ opposite-sign causal response from PWC$_u$ to Niño3.4 at ~~one~~ two season lag (~~Fig. 5a and~~ 1990-2010 in Fig. 3c) which might be an artifact of the seasonal variations of PWC.

Concerning the Atlantic-Pacific connections, the results suggest a clear decadal change in the interactions. In Fig. 3b, during the 1950-1970 and the 1960-1980 periods the ENSO effect on the tropical Atlantic SST modes is dominant. This is shown as a same-sign (positive cross-MCI) Niño3.4 → ATL3 link at lag zero and Niño3.4 → TNA at lag 1. The first two periods correspond to mainly negative PDV and AMV phases (see panel a). During the subsequent 1970-1990 period, where PDV switches to a positive phase after the mid-1970s and AMV is in a cold phase, the results show the emergence of a negative-sign response from ATL3 to PWC_u. We also notice during this period a weakening of the Niño3.4 links to TNA and ATL3, but an extra-tropical link to TNA is established through PNA (lagged PNA → TNA during 1970-1990). During the 1980-2000 and 1990-2010 periods, there is a decay of the same-sign influence from ENSO to the tropical Atlantic as no direct Niño3.4 → TNA nor Niño3.4 → ATL3 links were detected (Fig. 3b and c). Meanwhile, a strengthening of the ATL3 to PWC link is apparent during the last two periods as AMV trends toward and maintains a warm state. This suggests that as the Pacific and the Atlantic SSTAs fluctuate on the (multi)decadal timescale, changes in the interactions between modes of interannual variability are inextricable. These changes are not only confined to the tropics. In the extra-tropical region, a change in the connection between PNA and NAO is also detected. While this is detected as a same-sign contemporaneous unoriented adjacency (PNA o-o NAO) during the first 20-year window 1950-1970 (and not detected during the 1960-1980 period), this connection was estimated as contemporaneous negative during the three subsequent periods, as suggested by previous literature. The PNA-NAO connection was also found with a 4-season lag, which might be detected as a false positive due to the high correlation to the previous winter. In Fig. 3c, where the causal networks take into account the effect of subtracting MEM, we detect a similar pattern to Fig. 3b with small differences. Generally, a switch after the 1970-1990 period from a Pacific-dominated regime to an Atlantic-dominated one is maintained. Apart from the non-estimated Niño3.4 links to TNA and ATL3 during the first period, the most noteworthy differences after removing the externally forced signal are: i) a slightly stronger link for the extra-tropical route connecting PNA to TNA at 1-season lag during 1980-2000 in comparison to 1970-1990, and ii) no pronounced increase in the strength of the 1-season lagged ATL3 → PWC_u link between the 1980-2000 and 1990-2010 windows (compared to the same window periods when MEM was not subtracted, Fig. 3c vs b), suggesting contributions of external forcings. A decadal regime shift in the Pacific-Atlantic interactions falls in agreement with findings from previous studies (e.g. Meehl et al., 2020; Park et al., 2023b). We further analyze longer periods similar to the ones proposed in (Park et al., 2023b), namely the Pacific-driven period (1950-1983) and the Atlantic-driven period (1983-2014). The causal networks obtained through PCMCI+ are shown in Fig. 4 before (panels a and b) and after (panels c and d) removing the externally forced signal.

Pacific-driven period 1950-1983

The Pacific-driven 1950-1983 is found to be dominated by a same-sign effect from ENSO on ~~TNA~~ both TNA (1-season lagged) and ATL3 (lag zero). The effect on TNA is detected through both tropical and extra-tropical routes. During an El Niño event, the weakened Walker circulation allows an eastward shift in the maximum convection center from the Maritime Continent to the central equatorial Pacific. This tropical convection triggers a poleward-propagating Rossby wave, which extends into the midlatitudes, constituting the PNA pattern (Wallace and Gutzler, 1981; Hoskins and Karoly, 1981; Karoly, 1983). This teleconnection linking the equatorial and extra-tropical Pacific is detected as a lagged ~~positive~~ same-sign causal link from ~~PWC_u~~ Niño3.4 to PNA during 1950-1983 (Fig. ~~5a~~ 4a and c). The wave pattern associated with PNA contributes to the formation

of an anomalous low-pressure center over the southeast United States and the Caribbean. The presence of the PNA pattern results in anomalous southwesterly winds over the TNA region. The negative rainfall anomaly over the western Pacific and the Atlantic region, caused by the reversed Walker circulation during El Niño, plays a role in inducing this anomalous low-pressure center over the southeast United States. Additionally, the suppressed heating response in the Atlantic region, resembling the Gill-like pattern (Matsuno, 1966; Gill, 1980) ~~,~~ might explain the Niño3.4 → ATL3 contemporaneous positive link (Fig. 4a and c) and also contributes to the development of anticyclonic circulation and southwesterly wind anomalies over the TNA region (García-Serrano et al., 2017b; Jiang and Li, 2019). The combined effect of these extratropical and tropical routes leads to southwesterly wind anomalies that weaken the northeasterly trade winds, reduce evaporation, and induce SSTA warming over the TNA region (Trenberth, 1997; Wallace and Gutzler, 1981; García-Serrano et al., 2017b; Jiang and Li, 2019; Meehl et al., 2020; Casselman et al., 2021; Park et al., 2023b). The two routes for the ENSO effect on TNA, which is ~~enhanced~~ predominant during the 1950-1983 period, can be seen through the causal networks in Fig. ~~5a~~ 4a and c showing two ~~positive~~ same-sign (lagged) links from the Pacific to TNA: PNA~~→~~→TNA (1 season) and Niño3.4~~→~~→TNA (1 season). ~~The TNA →PNA link in Fig. 5a and c is lagged by two seasons which might suggest that the warming over the TNA region contributes back to anomalous southwesterly winds and maintains the PNA pattern. The~~

The Pacific-driven regime's causal ~~graphs show that after El Niño excites PNA, the latter appears to be mutually connected to the NAO with a 7-season lag (PNA→NAO and NAO→PNA links in Fig. 5a and c) . These links are however~~ graph when MEM is subtracted (Fig. 4c) shows a 4-season lagged PNA→NAO link, inconsistent with previous studies on the linkage between North Atlantic and North Pacific modes of atmospheric circulation ~~and which suggest contemporaneous negative links~~ that suggest the contemporaneous negative link between PNA and NAO. This 4-season lagged link, as mentioned earlier could be the artifact a spurious correlation to the next year's winter. Honda et al. (2001) conducted a study on the period between 1979 and 1994 and discovered a negative correlation (-0.7) between the intensities of the Aleutian and Icelandic lows (low-pressure centers of the PNA and NAO, respectively). Song et al. (2009) concluded that the strongest negative correlations between PNA and NAO occur with no time lag and within a range of 10-day lags. By analyzing reanalysis datasets, Pinto et al. (2010) found no significant anti-correlation between PNA and NAO between 1950 and the mid-1970s, but this was ~~clearly~~ detected during the sub-period 1973–1994. A period of weak PNA-NAO coupling might explain the undetected contemporaneous PNA~~→~~→NAO negative links during the Pacific-driven period (Fig. 4a) and the 1960-1980 window in Fig. 3b. According to Soulard and Lin (2016), it is the absence of tropical forcing from ENSO that strengthens the relationship between PNA and NAO. On the other hand, observational uncertainty ~~prior to~~ before the satellite era can also be a reason that lagged and/or positive links were detected between NAO and PNA (1950-1970 in Fig. 3b and c) instead of contemporaneous negative links. On the Atlantic side, apart from the influence of ENSO and PNA on TNA, NAO is also found to ~~impact the~~ be connected to TNA SSTAs (contemporaneous negative TNA→NAO and 1-season lagged TNA→NAO ~~→TNA~~links in Fig. ~~5a~~ 4a and c). ~~The~~ Proposed mechanisms for this connection involve changes in pressure gradients between the Azores high and the Icelandic low ~~can~~ which alter trade winds, heat fluxes, and SSTs. Reduced northeasterly trade winds contribute to trapping warm SSTAs over the TNA region as less latent heat is released into the atmosphere (Cassou and Terray, 2001; Lee et al., 2008). ~~We detect several causal connections between NAO and TNA where the NAO drives changes in TNA, not only contemporaneously but~~

also lagged (NAO→TNA, Fig. 5a and c). This negative relationship of the NAO index with TNA is seen through the negative NAO→TNA links in Fig. 5a and c. Although direct links Although a direct link connecting either Niño3.4 (or PWC_u) to NAO have not has only been detected during the Pacific-driven regime1950-1970 window (Fig. 3c), the NAO is thought to affect the interplay between ENSO and TNA which is further complicated by the fact that ENSO can also influence the NAO through extratropical pathways (García-Serrano et al., 2017a; Casselman et al., 2021). If we consider the causal links that connect the SST modes (Niño3.4 and TNA) directly, to TNA and/or ATL3) directly or through PWC_u and PNA, then these results support the hypothesis that it was the Pacific SSTs mainly driving the same sign same-sign response on the Atlantic SSTs between 1950 and 1983 (Meehl et al., 2020; Park et al., 2023b). Overallthe first half of the analyzed period 1950-2014 (Meehl et al., 2020; Park et al., 2023b). Most importantly, comparing Fig. 5a 4a to c reveals a limited effect of external forcing the emergence of a weak negative lagged ATL3 → PWC_u link when external forcing is removed during the first periodas no major changes were detected in the causal graph after subtracting MEM .. This might be due to MEM estimating a net cooling effect of external forcing on equatorial (and north tropical) SSTs during that period, which results in warmer ATL3 (and TNA) anomalies between 1950 and the mid-1980s when MEM is removed (see TNA and ATL3 time series in Fig. 1b and f, respectively).

Atlantic-driven period 1985-20141983-2014

During the second period, the monopole SSTA pattern centered over the TNA region (shown Unlike the first period, equatorial and north tropical Atlantic warming is observed during the second period (see TNA and ATL3 in Fig. 3d)suggests enhanced precipitation there1b and f, and AMV in Fig. 3a), bringing anomalous westerly wind and enhanced precipitation (Park et al., 2023a) . The Rossby wave energy associated with the enhanced increased precipitation propagates toward the subtropical tropical Pacific. Combined with the modulated Walker circulation, this induces easterly wind anomalies over the equatorial Pacific, favoring the development of La Niña events (Ham et al., 2013b; Park et al., 2022, 2023b). This Overall, during 1983-2014 the Atlantic Niño and TNA are hypothesized to have similar fingerprints concerning the effect on ENSO (Park et al., 2021). The Atlantic effect on ENSO is illustrated in Fig. 5b 4b and d through the 1-season lagged TNA→ATL3 →PWC_u strongly negative link, an effect that evidently reaches the Niño3.4 node (strong PWC_u→PWC_u →Niño3.4 link). The externally forced causal graph in Fig. 4b also features a weak 1-season lagged TNA→PWC_u which vanishes when MEM is removed (Fig. 4d). While the atmospheric bridge connecting the equatorial and the extra-tropical Pacific was detected as PWC_u→Niño3.4→PNA links in Fig. 5a-c, this was detected as a direct contemporaneous Niño3.4→PNA link when external forcing is removed 4a-c, this link was not detected during the second period (Fig. 5d). Without external forcing, the 4b and d). The NAO is found to drive small changes in TNA (Fig. 5d). The contemporaneous TNA-NAO connection is found in the opposite direction during the externally forced Atlantic-driven 4b and d), in contrast with the direction estimated during the Pacific-driven regime (TNA→ →NAO, Fig. 5b4a and c). The latter is also the strongest occurrence of TNA-NAO links among the results in Fig. 5. The ENSO PNA effect on TNA through the extratropical pathway is still detected when external forcing was not removed. This is seen in Fig. 5b as a contemporaneous link from PNA to TNA in addition to an extratropical PNA teleconnection through PWC_u anomalies (PNA→TNA and PWC_u →PNA links). This mild contemporaneous PNA →TNA link is suppressed when MEM is subtracted, in contrast to the appearance of a strong 8-season lagged PWC_u →NAO link is detected as a weak link in

Fig. 4b and stronger when external forcing was removed (Fig. 5d)inconsistent with the already proposed negative and short lagged ENSO-NAO relationship (Brönnimann et al., 2006; Brönnimann, 2007)4d). Contrary to the first period, the contemporaneous negative PNA connection to NAO (Honda et al., 2001; Song et al., 2009; Pinto et al., 2010) is detected during the second period (PNA →as a contemporaneous unoriented adjacency (PNA o-o NAO in Fig. 5b and NAO →PNA in Fig 5d4b and d). Song et al. (2009) explain the anti-correlation they found between day-to-day variability of the Aleutian low and Icelandic low being as the result of the anomalous Rossby wave-breaking events associated with the PNA pattern. The paper shows authors show that when the PNA is in a positive (negative) phase, there is more (less) Rossby wave breaking over the North Pacific (Atlantic), which can weaken or split (strengthen) the polar vortex over that region. This can then affect the jet stream and the storm tracks over the North Atlantic, leading to a negative (positive) NAO phase (Song et al., 2009). Lagged negative causal PNA→→NAO and NAO→PNA links are →PNA links were also detected during the 1985-2014 period. two windows spanning 1970-2000 in Fig. 3b and c.

It appears from Fig. 5 that external forcing does not have significant effects on the causal networks from the 1950-1983 regime (Fig. 5c vs 5a), consistent with the SST correlation maps suggesting no major difference before and after subtracting MEM period that the effect of MEM was to suppress a weak negative sign effect from ATL3 on ENSO through PWC (Fig. 3a 4c vs 4a). Whereas for the following 1985-2014 period, changes were only detected in the tropical/extra-tropical pathways connecting Atlantic and Pacific. The difference between Fig. 3d and 4d hints at a major role played by the externally forced signal in the negative relationship between the TNA index and the tropical east Pacific SSTAs during the Atlantic-driven regime, which is not clearly detected by comparing causal graphs (Fig. 5b vs 5d). Namely, the causal networks show the effect of external forcing as in TNA causing changes in NAO and also in establishing the extra-tropical PNA connection to TNA with no seasonal lag. The latter connection is suppressed when external forcing was removed, in contrast to the appearance of a lagged PWC_u →NAO link (comparing Fig. 5b and 5d). Most importantly, inconsistent with the correlation map in Fig. 4d, the one-season lagged negative TNA →PWC_u link was still detected, with similar strength (link coeff.), after removing the externally forced signal. It is important to note that this discrepancy, regarding the effect of removing MEM during 1985-2014, was less apparent during a sensitivity test we carried out. There, the analysis of the Atlantic-driven regime was started one year later (1986 instead of 1985) in the observational run and the respective causal graphs revealed that the negative sign response from TNA to PWC was not detected after removing MEM (Supplementary Fig. S1), consistent with the correlation maps from 1985-2014. This further supports the already proposed studies indicating an increasing impact of external forcing on North Atlantic SSTA changes and the associated widespread effects during the most recent decades (Murphy et al., 2017; Klavans et al., 2022; He et al., 2023). In Supplementary Fig. S1, the 8-season lagged PWC_u →NAO (featuring in Fig. 5d) was detected before and after subtracting MEM.

The variability of ENSO 's relationship to TNA 1983-2014 period, external forcing seems to favor a weak contribution of TNA to the predominant negative sign effect of Atlantic on ENSO. The non-stationary relationship of ENSO to the tropical Atlantic from one regime to another is influenced by the decadal changes in the background mean state. A study by Park and Li (2018) found that the relationship between ENSO and TNA SST is non-stationary and depends on the Special

emphasis needs to be given to the effect of AMV in the interplay between the Atlantic Niño and the tropical Pacific. The interconnection between AZM and ENSO is favored during the negative phase of the AMV ~~.~~ when a shallower thermocline enhances equatorial SST variability (Martín-Rey et al., 2014b; Park and Li, 2018). Furthermore, Wang et al. (2017b) propose an Atlantic capacitor mechanism, wherein ENSO impacts TNA through an atmospheric bridge (termed as "charging"). Subsequently, the Atlantic influences the following ENSO by "discharging" via a subtropical teleconnection. Specifically, when AMV is trending to its negative phase, the impact of ENSO on TNA becomes amplified and has a more prolonged effect (Park and Li, 2018) . This was the case during the first two analyzed windows in Fig. 3 and the 1950-1983 period in Fig. 4 when AMV was trending towards its negative phase. During the ~~1985-2014~~ following period, AMV was trending back from a negative to a positive phase and the opposite was observed (~~reduced amplitude and shortened effect~~decaying strength). The anomalously warm North Atlantic SSTAs during the positive AMV phase favor the strengthening of the PWC, which ultimately brings upwelled cold water to consequently cool down the central equatorial ~~pacific~~Pacific. The specific contributions of internal variability to these regime changes remain unclear. Zhang et al. (2019) emphasizes the influence of the thermohaline circulation, particularly the Atlantic Meridional Overturning Circulation (AMOC), on the multidecadal changes in Atlantic SSTs. ~~Whereas for~~ Their study also suggests that the interannual fluctuations ~~, the paper suggests they~~ are primarily driven by wind-induced changes in turbulent heat fluxes. On the other hand, a series of recent papers (Booth et al., 2012; Mann et al., 2014; Bellucci et al., 2017; Watanabe and Tatebe, 2019; Klavans et al., 2022) show growing evidence of an increasing effect of external forcing on the AMV and its lead/lag association with the AMOC. This ~~suggests~~ implies that internal variability and external radiative forcing contribute to the decadal SST variations over the Atlantic (Meehl et al., 2016; Park et al., 2019; Meehl et al., 2020; Klavans et al., 2022; Park et al., 2023b).

4.2 Pacemaker simulations

~~**Standardized indices from the Pacific pacemaker ensemble (10 members) together with observations (HadISST) for Niño3.4 (a) and TNA (b). The lines in black show the observed time series from HadISST data before (solid) and after (dashed) subtracting MEM (similar to Fig. 1). The red lines represent the CESM2 Pacific pacemaker ensemble average (10-members) before (solid) and after (dashed) subtracting MEM.**~~

4.2.1 Pacific pacemaker

To scrutinize the potential causal dependencies between the modes, we use a 10-member ensemble of the CESM2 Pacific pacemaker simulations (see Sect. 2.2) where ~~Eastern Tropical~~ tropical SSTAs have been nudged towards observed values (maintaining ENSO evolution, ~~Fig. 6a~~see Supplementary Fig. S4c). The rest of the coupled model is free to evolve, resulting in different climate variations outside the nudging region depending on the single realizations' ~~own~~ initial conditions. The range of possible outcomes for Atlantic SSTAs is then governed by contributions from internal variability, CMIP6 time-varying external forcing, and the potential cross-basin contributions from the Pacific according to the model's dynamics. The variations of the TNA ~~index in the pacemaker simulations are compared in Fig. 6b to observations (see legend top right),~~ and ATL3 indices in the Pacific pacemaker simulations before and after removing the CMIP6 time-evolving external forcing (MEM) ~~.~~ are

shown in Supplementary Fig. S4a and f, respectively. To illustrate the long-term state of the Pacific and Atlantic basins in the Pacific pacemaker ensemble, we show in Fig. 5a and b, the low-pass filtered PDV and AMV time series averaged across all ensemble members (shadings denote the 25th to 75th percentile range) where orange (blue) curves denote the ensemble time series before (after) subtracting MEM. The observed time series of both low-pass filtered indices before (after) subtracting MEM are shown as black (green) dashed lines. The PDV is defined north of 20°N and is outside the nudging region, and is the same for AMV in the Atlantic. This means that the SST in the PDV and AMV regions (see Sect 2.4) are free to evolve according to the CESM2 model coupling, CMIP6 external forcing, and the tapering applied. There are several discrepancies before the 1990s between the pacemaker-simulated and the observed indices (before and after subtracting MEM) for both PDV and AMV. However, Fig 5a shows that the 25th-75th percentile range of pacemaker-simulated PDV reduces significantly after the 1990s when external forcing is enhanced (orange shading in Fig. 5a). Removing external forcing brought PDV closer to the observed range of anomalies but with a wider range of values, i.e. restoring internal variability. The pacemaker-simulated AMV follows closely the observed range of anomalies before and after MEM is removed, especially after the 1990s. This further shows the increasing effects of external forcing in steering North Atlantic warming during the most recent decades of the analyzed period and the modulation of variability over the Pacific.

~~Figure 7 is similar to Fig. 5 but shows causal networks based on an ensemble summary of CESM2 Pacific pacemaker simulations. The causal networks are aggregated based on 10 pacemaker realizations. In the four panels (a-d) , we apply the PCMCI~~Similar to Fig. 3b and c, in Fig. 5c and d, we show a similar analysis applied to the Pacific pacemaker ensemble using the Multidata-PCMCI+ ~~on the time series of each simulation before aggregating. The link width indicates the number of simulations that feature that link (for reference, the width of the link between PNA and NAO in Fig. 7a shows the maximum width, equivalent to~~ function. For every window, the causal graph represents the average causal dependencies from all 10 ~~simulations, and the link between~~ ensemble members. As more samples are available for the Pacific pacemaker, we lower the significance threshold α_{pc} to 0.01 to show only robust (low uncertainty) links. We also note that the causal graphs shown in this section are subject to special assumptions (due to the nudging) as mentioned at the end of section 3.2.2. In most of the periods from the five analyzed windows in Fig. 5c, we see the same-sign effect of the Pacific on the Atlantic either through the tropical (Niño3~~.4 and TNA shows the minimum width, equivalent to 2 simulations) . In other words, the more ensemble members were found to estimate the link during that particular run, the thicker the link appeared. The mean link coefficient value averages all coefficients of that link's instances and the link labels denote the median time lag at which they were detected. The node color translates the average auto-link coefficient of each time series among the pacemaker ensemble.In Fig. 7c and d, the MEM is subtracted from every simulation before the causal discovery algorithm is applied. For simplicity, we directed contemporaneous linksbased on the most frequent direction in which they are detected within the ensemble (treating each period and scenario separately) . We also only took into account links with absolute value coefficients above the arbitrary threshold of 0.1.~~ .4→TNA) pathway or the extra-tropical one (PNA→TNA) or both. This is also true after subtracting MEM (Fig. 5d).

The prominent feature of the causal analysis on the Pacific pacemaker simulations before removing external forcing (Fig. ~~7a and b~~5c) is the ability to distinguish a ~~Pacific-driven period as opposed to an Atlantic-driven one. Similar to observations, the~~

regression and correlation maps in Fig. 3 and 4, and previously introduced literature (Meehl et al., 2020; Park et al., 2023b), the causal networks in Fig. 7 also show the 1950-1983 period was dominated by the period with an Atlantic effect on PWC-related wind anomalies. All periods after 1950-1970 show the equatorial Pacific SSTAs driving a same-sign effect on the tropical North Atlantic SSTAs and TNA SSTAs (and ATL3 during the last window) and triggering a negative-sign response from the Atlantic onto the Pacific during the subsequent 1985-2014 period most recent periods when external forcing is strongest (via TNA$\rightarrow\rightarrow$ PWC$_u$). This is illustrated during the first period through the links originating from the Niño3.4 (and/or the PWC) node and reaching the Atlantic modes (NAO and/or TNA nodes) either directly (e.g. PWC– TNA) or potentially through PNA (Niño3.4 $\rightarrow$ PNA $\rightarrow$ NAO, Fig. 7a-c). Both the results from the reanalysis (Fig. 5a) and those from the pacemaker ensemble (Fig. 7a) show positive causal Niño3.4 $\rightarrow$TNA links and/or PWC$_u$ $\rightarrow$TNA during the Pacific-driven 1950-1983 regime. When MEM is subtracted during this regime (Fig. 7c), contemporaneous PNA $\rightarrow$TNA links were also estimated. This means that both the tropical and extra-tropical routes for ENSO effect on TNA are detected during the Pacific-driven regime (Fig. 7a and c). The 1985-2014 period knows a decay of the extra-tropical pathway (no PNA $\rightarrow$TNA link The two last windows in the panel c also show a decay of ENSO's same-sign effect accompanied with detection of lagged negative links from tropical Atlantic SSTA to PWC. Unlike observations, removing external forcing in Fig. 7b) and shows that several ensemble members detect rather the negative TNA $\rightarrow$PWC$_u$ link, which is consistent with the causal network from reanalysis (Fig. 5b). The thick line of the TNA $\rightarrow$PWC$_u$ connection in Fig. 7b suggests that most of the CESM2 pacemaker simulations with nudged observed SSTAs in the equatorial Pacific simulate the opposite-sign response from the Atlantic to the Pacific during the Atlantic-driven 1985-2014 regime before subtracting MEM. In the meantime, the positive-sign impact from the Pacific on the Atlantic (via either Niño3.4 or PWC on TNA)was detected by at least two members in each experiment. For example, 5d results in the complete disappearance of TNA$\rightarrow$ PWC$_u$. This suggests that in the Niño3.4 $\rightarrow$TNA link appears in the four experiments (all panels in Fig. 7). This link is more evident when MEM is subtracted during the second period as Fig. 7d shows more ensemble members to simulate the link (thicker Niño3.4 $\rightarrow$TNA link) compared to Fig. 7bPacific pacemaker ensemble, the Atlantic might have played an essential role in modulating the effects of external forcing during the 1990s and early 21st century by modifying the Walker circulation (inducing easterly wind anomalies). Literature suggests that ENSO (Maher et al., 2015, 2018) and its decadal imprint, PDV (Allen et al., 2014; Dong et al., 2014), have contributions from external drivers, especially volcanic and anthropogenic aerosols. Other studies show that recent period of global warming hiatus is the result of anthropogenic aerosols modulating the phase of PDV rather than canceling out other warming effects (Kaufmann et al., 2011; Smith et al., 2016).

The simulations from the pacemaker ensemble agree greatly are in agreement with the proposed contemporaneous negative PNA relationship to NAO (Honda et al., 2001). This was mostly detected as contemporaneous PNA$\rightarrow$NAO links in Fig. 7a-c and as NAO $\rightarrow$PNA in Fig. 7d. As can be seen from Fig. 7, the similarities with the causal networks from observational data (Fig. 5) entail an important role of ENSO (in combination with external forcing) in shaping SST variability over the Atlantic. While the PNA-NAO connection is found positive and lagged in observations during the 1950-1983 period (Fig. 5a and c), it is detected as a negative contemporaneous connection in most pacemaker simulations . Removing external forcing for the Pacific-driven 1950-1983 regime did not have a significant effect in the case of reanalysis and the same for the pacemaker ensemble except for the vanishing PWC$_u$ $\rightarrow$TNA link. The relationship between ENSO and PNA is, however, detected by

fewer simulations when removing external forcing , and it is illustrated in Fig. 7c by a thinner and weaker (on average) positive Niño3.4 →PNA link compared to the one in Fig. 7a →NAO or PNA o-o NAO links. The importance of both ENSO and external forcing is further manifested during the 1985-2014 period through the emergence of the negative sign effect While this section provides insight onto the effects of ENSO and external forcing in the interaction between the two basins, the next section provides the results of a similar analysis using an ensemble of Atlantic pacemaker simulations to investigate the combined effects of the Atlantic and external forcing on the Pacific.

4.2.2 Atlantic pacemaker

Similar to section 4.2.1, Fig. 6 shows the PDV and AMV time series (panel a and b) and the Multidata-PCMCI+ results from the Atlantic (TNA)on the pacemaker ensemble (panel c and d). While there are notable differences between the Atlantic pacemaker-simulated and observed PDV, these differences are reduced significantly after the 1990s. In the North Atlantic, small differences between the observed and Atlantic pacemaker-simulated AMV are mostly due to observational uncertainty (HadISST vs ERSSTv3b). As mentioned earlier in this section, we assume links only originate from the Atlantic affecting the Pacific (Niño3.4 through PWC), similar to the observations (Fig. 5b). On the other hand, when subtracting MEM from the pacemaker simulations, more members show the positive Niño3.4 →TNA link (Fig. 7d) while the significant negative TNA → PWC_u link is not detected (Fig. 7d vs . 7b). We recall that this is different in the causal networks from the observed 1985-2014, which feature the negative TNA →PWC_u before and after subtracting the MEM (north Atlantic SSTAs nudged toward observations). Similar to observations (Fig. 3) and the Pacific pacemaker ensemble (Fig. 5b and d) . This apparent effect of external forcing being the main driver of an Atlantic-driven regime during the second period is nevertheless implied by the results from the correlation/regression analysis in the previous section (5), the results in Fig. 4d vs 3d)and the sensitivity test in Supplementary Fig. S1. Subtracting external forcing during the most recent period resulted in a change in the direction of the link between PWC_u 6 demonstrate that the same-sign response between TNA and Niño3.4 and the link between NAO and PNA. As the directions of contemporaneous links were decided by majority rule (the most frequent direction of a particular lag-zero link among all ensemble members during a specific run), Fig. 7d shows that more ensemble members detected those links in the opposite direction (Niño3.4 → PWC_u and NAO →PNA) .

The observed Niño3.4 time series in Fig. 6a is similar to the pacemaker ensemble mean (because SSTAs over the Niño region are nudged towards observed values; small differences, most likely originating from observational uncertainty, ERSSTv5 vs HadISST). The pacemaker ensemble mean TNA (red lines is detected during the first three windows spanning from 1950 to 1990 and decays afterward. Additionally, the negative sign effect of the tropical Atlantic on PWC (and ultimately ENSO) is prevalent throughout all analyzed periods (except the first window in Fig. 6b)implies an important role of ENSO in shaping SSTAs over the Atlantic, possibly through combining internal variability processes and modulating the effects 6c), with little difference before and after subtracting MEM. This suggests that internal variability alone can generate the decadal change in the interactions between the Pacific and the Atlantic. Nevertheless, there are small contributions that appear to be the result of external forcing . Despite several discrepancies between the observed and the pacemaker-simulated TNA indices during the years following major volcanic eruptions (e.g. the early 1990s) and during important El Niño / La Niña events (e.g. 1997–1998)

and are illustrated through slightly stronger opposite-sign links during 1970-1990 (ATL3 → PWC$_u$) and 1990-2010 (TNA → PWC$_u$) when the externally forced signal is kept (Fig. 6c). An interesting feature is that as the PDV switches to a negative phase after the 1990s, the ~~pacemaker ensemble follows similar variations to the observed TNA through most of the 1950 to early 2000s period (red solid and dashed lines compared to black lines). The fact that prescribing SSTAs only in the equatorial Pacific resulted in TNA SSTAs similar to observations emphasizes the role of ENSO in the Atlantic-Pacific interactions and undermines the role of internal variability in driving SST variability over the Atlantic during most of the analyzed period. Literature suggests that ENSO (Maher et al., 2015, 2018) and its decadal imprint, PDV (Allen et al., 2014; Dong et al., 2014), have contributions from external drivers, especially volcanic and anthropogenic aerosols. Other studies show that recent periods of global warming hiatus are the results of anthropogenic aerosols modulating the phase of PDV rather than canceling out other warming effects (Kaufmann et al., 2011; Smith et al., 2016). The results~~ negative sign impact of the Atlantic on PWC becomes mainly detected from TNA and not ATL3 (Fig. 6c,d). In the Atlantic pacemaker ensemble, this feature seems to be independent of the AMV phase as there are considerable differences in the magnitude of the AMV index before and after subtracting MEM (orange vs blue time series in Fig. ~~7 also suggest that the coupling between Atlantic and Pacific SSTs is moderately strong in the CESM2 model during Niño events, explaining the appearance of Niño3.4 →TNA (and/or PWC$_u$ →TNA) links in all causal networks on Fig. 7 (a-d). This also explains the large discrepancies between the pacemaker ensemble mean (lines in red) and observations (lines in black) in Fig.~~ 6b~~during significant El Niño years. The main difference between the reanalysis and pacemaker causal networks remains during the Atlantic-driven regime after removing external forcing. Figure 6b shows increasing differences between the observed and the pacemaker-simulated TNA after the year 2000. This difference might be due to the overestimation of the 1998-2013 global warming rate in~~), but not pronounced discrepancies between causal graphs of Fig. 6c vs d. We note that the directions shown for the contemporaneous connections with TNA are based on assumption 8 discussed in Sect. 3.2.2 (i.e. based on the nudging). Causal graphs obtained when no assumption is introduced during the analysis of the Atlantic pacemaker ensemble are shown in Supplementary Fig. S13.

An important consideration is the difference in the externally forced signal between the Atlantic pacemaker simulation and MEM. Unlike the Pacific pacemaker ensemble and MEM, the externally forced signal in the Atlantic pacemaker simulations is based on the CESM1 model, which includes CMIP5 (and not CMIP6~~climate models(McBride et al., 2021; Smith et al., 2021; Fyfe et al., 2~~ ~~, and inherently in MEM. Different factors contributing to such overestimation in~~) forcing. The same estimate of external forcing (MEM based on CMIP6 ~~have been proposed including the high equilibrium climate sensitivity (ECS) that results in too strong warming responding to anthropogenic GHGs or too weak cooling responding to aerosols (IPCC, 2013; Tokarska et al., 2020a; Schlun~~ ~~. According to Wei et al. (2021), ECS only plays a partial role in the failure of most~~ large ensemble models) is removed from both pacemaker ensembles. This presents a limitation to the assessment of external forcing on the CESM1 model in this section. On the other hand, consistency in the estimation of MEM as the forced signal at least addresses the issue of major differences due to volcanic aerosol forcing in the second half of the 19th century and early 21st century. These differences have been reported and mainly attributed to small-to-moderate eruptions included in CMIP6 ~~models in simulating the early 2000s global warming slowdown. Instead, the authors attribute the discrepancy between observed and CMIP6-simulated warming trends mostly to the models' deficiencies in simulating major modes of internal variability at interannual, interdecadal, and~~

multidecadal scales, thus excluding their potential effects (e.g. the cooling effect of PDV switching to a negative phase in the early 2000s).

natural forcing but not in CMIP5 simulations (Fyfe et al., 2021). The different sources of external forcing , as well as the overestimation of most recent warming trends, and the coincidence of volcanic eruptions with ENSO events complicate the complicate the precise attribution of external contributions to the Atlantic-Pacific interactions during the last decades of the historical record. To further test whether the observed teleconnections (including a change in the regime of Atlantic-Pacific interactions) would arise only from internal climate variability (and natural external forcing), the next section presents results from a pre-industrial control run of the CESM2 model.

4.3 Pre-industrial control simulations

Given 120 years of unforced simulation, we use In the absence of anthropogenic forcing, Atlantic-Pacific interactions inherently depend on the mean state of the two basins. To illustrate this, we use 250 years (3-monthly averaged, 1000 times steps) from the CESM2 pre-industrial run to analyze the causal connections between the Atlantic and Pacific during their different states. (CESM2 piControl). In Fig. 7 a-d, the PCMCI+ causal graphs are shown for specific phase combinations depending on the sign of the low pass filtered (13-year Lanczos) time series of PDV and AMV shown in Fig. 7e.

Figure 8a shows the long-term state of the two basins through the smoothed time series of AMV (solid; red and blue) and PDV (dashed; pink and light blue) indices from 120 years of CESM2 First, most of the observed teleconnections (and pacemaker-simulated) are also detected during the pre-industrial control simulation, precisely from the start of the year 1000 to the end of 1 We define three 40-year periods (160 seasons each) and we reconstruct a causal network for each that represents the connections between the Atlantic and Pacific basins. We investigate such periods the same way we did for reanalysis data and the Pacific pacemaker simulations in Sect. 4.1 and 4.2, respectively, focusing on the links between the Atlantic and Pacific modes. The causal graphs initially displayed several links of different link strengths. Here in Fig. 8b, we show only the strongest links (with absolute value link coefficients above the arbitrary threshold of 0.15; i.e. enhanced link colors).

The first 40-year period in Fig. 8a (P1)corresponds to PDV mainly in a positive phase while AMV is trending from a negative to a neutral state. During this period run. The same-sign effect of the Pacific on the Atlantic is estimated during three out of the four regimes. During PDV+/AMV+, PDV-/AMV+, PDV+/AMV- (Fig. 7a-c), it is detected as both tropical pathway from Niño3.4 SST changes were found to strongly affect the PWC-associated zonal winds (1 season lagged positive Niño3.4 →PWC(and PWCu) to TNA and/or ATL3 (1-2 season lag), and extratropical route from PNA to TNA (0-1 season lag). On the other hand, the negative sign effect of the Atlantic on the Pacific is detected from ATL3 to PWC_u link; P1 in Fig. 8b) . These wind-induced changes are detected to affect extra-tropical PNA mode with a 1-season lag (positive PWC_u →PNA). The PNA changes are detected to be affected by NAO changes as well (NAO →PNA). The causal graph shows that the Pacific was contributing to tropical North Atlantic SSTA changes mainly through the extra-tropical pathway, detected as a contemporaneous positive PNA →TNA link, where the lower pressure center at the southeastern lobe of the PNA pattern reduces the Atlantic northeasterlies, trapping warm water over the TNA region. only when PDV is in a negative phase (PDV-/AMV+, PDV-/AMV-, Fig. 7b and d).

~~The second period (P2 in~~ Moreover, the results also show that the two basins are "better" interconnected when PDV and AMV are out of phase (PDV-/AMV+, PDV+/AMV-; Fig 7b and c) as there are more links with higher cross-MCI values compared to when the two indices (AMV and PDV) are in phase i.e. PDV+/AMV+ and PDV-/AMV- (Fig. ~~8a)illustrates a mostly positive AMV (trending negative towards the end of P2) while the~~ 7a and d). Specifically, the same-sign effect of ENSO on tropical Atlantic SSTAs is more pronounced when the decadal North Pacific SSTA is in a warm state while the North Atlantic is in a cold state (PDV~~switches from a negative to a positive phase . The causal graph (P2 in Fig . 8b) features a positive Niño3.4 →PNA link and a strong negative contemporaneous PNA →NAO link. The ENSO-induced changes are also found to contribute to the TNA SST anomalies (positive Niño3.4 →TNA link). Both tropical (Niño3.4 →TNA) and extra-tropical (Niño3.4 →~~+/AMV-, Fig. 7c). Conversely, when these phases are inverted (PDV-/AMV+), it is the extra tropical atmospheric variability modes that are strongly connected (PNA ~~→NAO →TNA) routes suggest the Pacific was mainly driving the Atlantic during this period.~~

~~The third period (P3 in Fig. 8a) shows PDV trending from a strong positive phase to a strong negative phase while the AMVcurve shows mainly positive SSTAs. The corresponding causal graph (P3 in Fig. 8b)shows that the warm TNA SSTAs strongly contributed to La Niña conditions over the Pacific through strengthening the PWC (strong negative 4-season lagged TNA →PWC_u link), cooling the Pacific on the decadal timescale (see PDV during P3 in Fig. 8a~~o-o NAO, Fig. 7b). The ~~warming SST trends in the Atlantic favor a strengthened PWC which ultimately cools the SSTs over the Niño3.4 due to enhanced upwelling. The effect of the Atlantic on the Pacific during this period is manifested in the extra-tropics as well where NAO is found to strongly contribute to PNA variability (contemporaneous NAO →PNA link) .~~ absence of strong El Niño forcing during that regime might explain the strength of the PNA-NAO in Fig. 7b, as suggested by Lin and Derome (2004); Soulard and Lin (2016) .

~~The PNA →NAO connection is stronger in P2 compared to~~ In contrast to the reanalysis and Pacific pacemaker ensemble, the causal graphs from the CESM2 piControl run show only instances of NAO contributing to TNA and not the other way around, suggesting stronger dependence of tropical North Atlantic SST on atmospheric variability forcing given the 250 years of unforced simulation. Another discrepancy is that the in-phase combination of AMV and PDV (PDV+/AMV+ or PDV-/AMV-) seems to be favored and long-lasting during the pre-industrial era in comparison to observations. During the finite sample of CESM2 piControl used here, AMV and PDV were in phase 58% of the time, but in observations (ERSSTv5) and the ~~NAO →PNA links in P1~~ CESM2 historical simulations (11 ensemble members) only 43% and 20% respectively, between 1900 and ~~P3. The relatively weak magnitudes of PDV anomalies during P2 (compared to P1 and P3; Fig, 8a) suggest reduced ENSO amplitude and hence limited ENSO-like tropical forcing during that period (despite the lagged Niño3.4 →PNA)~~ 2014 according to (Karmouche et al., 2023). Does the external forcing signal observed during the historical period drive an "unstable" state where contrasting responses between the two basins are favored due to the prevalence of an out-of-phase regime? To answer this question, longer periods and more CMIP6 large ensemble models with historical simulations and their pre-industrial counterparts should be analyzed. ~~The absence of strong El Niño forcing might explain the strength of the PNA connection to NAO in P2, as suggested by Lin and Derome (2004); Soulard and Lin (2016).~~

~~What can be concluded from~~ From the analysis of the pre-industrial run, the following could be summarized~~as follows~~: (i) "Pacific-driven~~and~~ " and "Atlantic-driven~~regimes, and the phase switch between them,~~ " periods happen naturally in the

absence of anthropogenic forcing. (ii) This does not reject the possibility that human-induced forcing contributed greatly to at least the observed ~~1985-2014 changes~~ changes after the 1990s. (iii) The strength, ~~direction, and lags~~ sign, and direction of the cross-basins ~~' seasonal-to-interannual~~ interactions are modulated by the long-term state of ~~the two~~ both basins (PDV and AMV).

5 Discussion and Conclusions

Serving as a "proof of concept" within the domain of comprehending complex climate phenomena, the El Niño event of 1997/1998 presents a notable example showcasing the efficacy of causal discovery in discerning the underlying drivers that govern well-established connections among contributing coupled processes (methods, Sect. 3.2.1). Hereupon, the scope extends beyond ENSO, delving into the less-explored topic of Atlantic-Pacific interactions. ~~Conventional regression and correlation methods offered indications of a regime shift in the Atlantic-Pacific interactions during the observed historical 1950-2014 period (Meehl et al., 2020; Park et al., 2023b). The correlation maps also showed that external forcing (represented by CMIP6 MEM) likely played a major role in setting the negative sign for the relationship between the TNA index and north tropical Pacific SSTAs during the Atlantic-driven 1985-2014 period (Fig. 4d vs 3d). However, these approaches could not explore the underlying pathways of these effects, which causal graphs provide by uncovering intricate causal relationships.~~

Based on causal graphs derived from reanalysis data and Pacific pacemaker simulations before and after separating the externally forced signal (~~a and b in Fig. 5 and 7~~Figs. 3-5), we find the Pacific's ~~same sign influence on Atlantic during 1950-1983~~same-sign influence on the Atlantic during the first half of the analyzed period, aligning with prior ~~reports~~ studies (Meehl et al., 2020; Park et al., 2023b). Estimated positive links from Niño3.4 (or PWC_u) to TNA (or ATL3) represent the tropical pathway where El Niño and the modified Walker ~~Circulation~~ circulation prompt equatorial Atlantic anticyclonic activity, weakening trade winds, and warming ~~tropical~~ tropical North Atlantic as a result of reduced evaporation. Other pathways recognized through PNA and NAO have also been detected. Positive causal links Niño3.4~~(or PWC_u)~~ $\rightarrow\rightarrow$PNA and PNA$\rightarrow\rightarrow$TNA highlight the extra-tropical path for the Pacific-induced effect on TNA. El Niño-associated Rossby wave propagation enhances Southeast United States low-pressure center (positive PNA phase), weakening North Atlantic trade winds and promoting TNA warming (Klein et al., 1999; García-Serrano et al., 2017b; Jiang and Li, 2019). The transition from a Pacific-driven to an Atlantic-driven regime is evident in reanalysis and ~~Pacific pacemaker simulations . During 1985-2014, causal graphs~~ pacemaker simulations through the weakening (or decay) of the same-sign response between ENSO and tropical Atlantic in the second half of the analyzed period (e.g. Fig. 3 c and d), accompanied by the emergence and strengthening of ATL3's and TNA's negative sign effects on PWC_u (Fig. 3 c and d, 5c). Based on reanalysis data, the 1983-2014 causal graphs (Fig. 4b and d) reveal lagged negative ~~TNA$\rightarrow$PWC~~ATL3$\rightarrow PWC_u$ and TNA$\rightarrow PWC_u$ links, denoting intensifying easterly trade winds affecting ENSO. Proposed mechanisms involve modified Walker circulation in the equatorial Atlantic for the effect of ATL3 (AZM) on PWC and the Rossby wave energy generated by enhanced precipitation ~~over~~ for the effect of anomalously warm TNA ~~region, impacting subtropical Pacificand causing~~ on the subtropical Pacific, which causes easterly wind anomalies and La Niña-like cooling (Wang et al., 2017b; Park and Li, 2018; Park et al., 2022). ~~Similar to reanalysis~~

data, Pacific pacemaker simulations distinguish Pacific and Atlantic-driven regimes in SST responses (directly or via PWC). In the meantime, pacemaker-simulated SLP-based indices denote negative contemporaneous Observations show a negative contemporaneous NAO-PNA relationship during 1950-1983 and 1985-2014. Notably, reanalysis identified positive 7-season lagged causal links during the first period, for which mechanisms are unclearrelationship only starting the 1970-1990 window (and the 1983-2014 period in Fig. 4). Earlier research proposed a robust negative correlation between Aleutian and Icelandic lows only during specific historical sub-periods (e.g., mid-1970s to mid-1990s; Honda et al., 2001; Pinto et al., 2010). This might clarify the absence of contemporaneous negative PNA-NAO links during the causal analysis for the Pacific-driven periods in reanalysis (Fig. 4a and c). Conversely, the simultaneous negative PNA-NAO link was consistently identified across both pacemaker ensembles and the pre-industrial control runs. This link could be the result of Rossby wave-breaking events connecting PNA to opposite NAO phases (Song et al., 2009) or simply because, particularly in certain seasons, the two modes are spatially overlapping projections of the same variability pattern, connecting the Aleutian and Icelandic lows (Soulard and Lin, 2016) .

The study involved A new aspect of the nature of Atlantic-Pacific connections is shown by separating external forcing from internal variability by subtracting CMIP6 MEM in the causal analysis, yielding insights into external forcing's impact on Pacific-Atlantic interactions. Although MEM removal had modest effects on Pacific-driven regime the Atlantic pacemaker causal graphs (panel c vs. a; Fig. 5 and 7Fig. 6b vs c), pronounced impacts emerged in the following period (panel b vs. d; Fig. 5 and 7), aligning with correlation and regression maps (Fig. 4d vs. 3d). During the Atlantic-driven era (1985-2014), reanalysis graphs highlighted TNA's strong contribution to same-season NAO changes (during the analysis of the Pacific pacemaker ensemble (Fig. 5b), reversed after MEM subtraction (Fig. 5d). Additionally, a shift in the extra-tropical route linking the Pacific and Atlantic was observed during that period. Importantly, a negative TNAto ENSO response (via PWC) persisted despite MEM removal. In contrast, aggregated pacemaker graphs underscored vs c), especially during the most recent periods. The 1980-2000 and the 1990-2010 periods in the Pacific pacemaker results show the emergence of ATL3$\rightarrow$PWC$_u$ and TNA$\rightarrow$PWC$_u$ only when the external forcing is not separated, underscoring external forcing's primary role in the Atlantic-driven regime, as evidenced by the vanishing TNA to PWC link and the emergence of Pacific-driven causal links after external forcing was removed. We note that the discrepancy between reanalysis and pacemaker aggregated causal graphs regarding the effect of subtracting MEM during 1985-2014 lessened when conducting a sensitivity test. Initiating the Atlantic-driven regime a year later (1986 instead of 1985) post-1980s periods. In contrast, the negative "ATL3 to ENSO" effect (via PWC) persisted through the second half of the analyzed period despite MEM removal in the reanalysis yielded no detected negative TNA $\rightarrow$PWC$_u$ link after MEM removal (Supplementary Fig. S1), in line with correlation maps and aggregated pacemaker graphs for 1985-2014. run (Fig. 3b vs c and Fig. 4b vs d). A major role played by external forcing in the negative effect of TNA on ENSO falls in agreement is consistent with recent studies highlighting an increasing impact of external forcing on North Atlantic SSTAs and associated effects in recent decades (Murphy et al., 2017; Klavans et al., 2022; He et al., 2023). This brings additions to additional insights into the debate over the attribution of the recently observed strengthening of the PWC, i.e. we suggest . Our results show that external forcing contributions modulated by the Atlantic might have amplified the recent PWC strengthening, in contrast with previous studies suggesting a dominant

role of internal variability (Chung et al., 2019). ~~Major disparities between observed and CESM2 pacemaker-simulated TNA indices (during the Atlantic-driven period) were discussed in Sect. 4.2 and attributed to the extensively investigated post-2000s warming overestimation in CMIP6 (Tokarska et al., 2020b, a; Smith et al., 2021; Fyfe et al., 2021; Smith and Forster, 2021). The pacemaker-simulated TNA index (Fig. 6b) time series revealed a moderately strong coupling in the CESM2 model between Atlantic and Pacific SSTs, resulting in major differences in magnitude with the observed TNA following important El Niño events. This might explain the appearance of Niño3.4 →TNA (and/or PWC$_u$ →TNA) links in all aggregated causal networks in Fig. 7 (a-d).~~

The analysis of the historical record (~~1950-2014~~from 1950 to early 21st century) suggests external forcing's potential contributions, yet doesn't exclude the role of internal variability driven by the Pacific and Atlantic long-term states (PDV and AMV). To explore Atlantic-Pacific internal variability interactions in unforced conditions, we ~~utilized 120~~ analyzed 250 years from the CESM2 pre-industrial control run, ~~divided into three 40-year periods. During two periods (P1 and P2), the~~ following a regime-oriented approach. The causal graphs underscore the Pacific's impact on ~~TNA~~ tropical Pacific variability through the tropical and extra-tropical pathways ~~. Whereas for the third period (P3), characterized by a predominantly positive AMVand a significant PDV phaseswitch, a robust lagged negative TNA →~~during three out of four regimes (all except PDV-/AMV-). The interconnection between the Atlantic and Pacific basins was found strongest when the PDV and AMV are out of phase (PDV+/AMV-, PDV-/AMV+), with more links and higher cross-MCI values compared to when they are in phase. Additionally, the negative sign effect ATL3→PWC$_u$ ~~link was evident, similar to Atlantic-driven regime causal graphs in reanalysis (Fig. 5b and d) and pacemaker simulations with externally forced signal (Fig. 7b). The lag for the TNA effect on PWC differs between the~~ was only detected when PDV was negative. The pre-industrial control ~~run (four seasons in P3) and observations/pacemaker ensemble (one season). In short, our pre-industrial control~~ analysis indicates that both contrasting response regimes arise naturally without anthropogenic external forcing, influenced by the long-term states of the Pacific and Atlantic basins.

~~Throughout this study, causal discovery revealed varying signs and lags for the links between PNA andNAO. Earlier research proposed a robust negative correlation between Aleutian and Icelandic lows only during specific historical sub-periods (e.g., mid-1970s to mid-1990s; Honda et al., 2001; Pinto et al., 2010). This might clarify the absence of contemporaneous negative PNA →NAO links during the causal analysis for the Pacific-driven 1950-1983 era in reanalysis (Fig. 5a and c), where lagged positive connections were observed. However, prior studies haven't outlined mechanisms for such multi-season lagged positive associations. Conversely, the simultaneous negative PNA-NAO link was consistently identified across pacemaker and pre-industrial control runs. This link could be the result of Rossby wave-breaking events connecting PNA to opposite NAO phases (Song et al., 2009) or simply because, particularly in certain seasons, the two modes are spatially overlapping projections of the same variability pattern, connecting the Aleutian and Icelandic lows (Soulard and Lin, 2016)~~The results in Figs. 5-7 suggest that the coupling between Atlantic and Pacific SSTs is moderately strong in the CESM models, explaining the appearance of links connecting Niño3.4 (and/or PWCu) to TNA (and/or ATL3) in most causal networks shown in Sect 4.2 and Sect. 4.3. The coupling is also realistic as it captures the observed patterns of interdependencies shown in Fig. 3. The main difference between the reanalysis and Pacific pacemaker causal networks remains during the most recent decades after removing external forcing. Differences might be due to the overestimation of the 1998-2013 global warming rate in CMIP6 climate models (McBride et al., 2021; Smith et al., 202

, and inherently in MEM. This additionally complicates the separation of external forcing in the CESM1 Atlantic Pacemaker ensemble as it includes CMIP5 forcing. Different factors contributing to such overestimation in CMIP6 have been proposed, including the high equilibrium climate sensitivity (ECS) that results in too strong warming responding to anthropogenic GHGs or too weak cooling responding to aerosols (IPCC, 2013; Tokarska et al., 2020a; Schlund et al., 2020; Smith and Forster, 2021; Wei et al., 2 . According to Wei et al. (2021), ECS only plays a partial role in the failure of most CMIP6 models in simulating the early 2000s global warming slowdown. Instead, the authors attribute the discrepancy between observed and CMIP6-simulated warming trends mostly to the models' deficiencies in simulating major modes of internal variability at interannual, interdecadal, and multidecadal scales, thus excluding their potential effects (e.g. the cooling effect of PDV switching to a negative phase in the early 2000s).

In a concluding remark, the authors would like to highlight that causal discovery is a powerful tool to assess the physical mechanisms of Atlantic-Pacific interactions. However, a careful selection of the potential variables representing the analyzed mechanisms and the length of the time series are crucial for a robust application of causal analysis and reliable interpretation of detected connections. ~~We experienced issues such that the algorithm rejected/added some connections when the analyzed period was prolonged or shortened and/or shifted by a few years.~~ Therefore in order to make credible conclusions based on the application of causal discovery, it is important to accurately determine the causal assumptions, clarify the correct confounding variables, and analyze the physically consistent interactions at their most relevant time scales to achieve robust results.

We also recognize the potential benefits of a more granular analysis, such as splitting each time series into four quadrants (representing four seasons) to analyze the effects on a particular season (e.g. on the peak season of a certain variable or summer vs winter periods). However, implementing such a quadrant-based method would dramatically shorten the data frame and impair the causal analysis, especially for reanalysis and pacemaker ensembles (where short periods are analyzed). Despite this limitation, the adopted methodology which considers the complete-year time series (3-monthly averaged) identifies the overall effect considering all time steps (seasons) and provides valuable insights into the seasonal lag and strength of causal relationships. Naturally, the most significant links (under the α_{pc} threshold) are the ones that come out on the causal graph, and which should always be interpreted according to background knowledge (e.g. with respect to the peak season of the variables analyzed). Given the complexity of causal graphs, the existence of prior knowledge about underlying physical processes can significantly improve the analysis and interpretation of the results. Therefore, the integration of expert assumptions helps avoid conflicting adjacencies to further estimate the strength of the connections.

Finally, this study aims to enhance our understanding of the teleconnections between the Atlantic and Pacific oceans and their variability under different regimes. The findings emphasize the significance of external forcing, particularly in the most recent regime, and highlight the roles of ~~ENSO,~~ tropical and extra-tropical pathways, and internal variability in shaping SST variability over the ~~Atlantic on seasonal to interannual~~ Pacific and Atlantic basins on different timescales. Further research is warranted to refine our knowledge of these complex interactions and improve model simulations to capture the observed teleconnections more accurately. External forcing represented by the CMIP6 MEM has contributions from natural (e.g. solar radiation, volcanic eruptions) and anthropogenic sources (e.g. aerosols, GHGs) with time and space-varying effects~~, hence,~~ .

Therefore, we encourage further analysis using simulations with single external forcing sources (e.g. aerosol-only or GHG-only simulations) to increase the understanding and attribution of the observed changes in the climate system.

Code and data availability. The CESM2 Pacific pacemaker ensemble dataset can be found here: https://www.earthsystemgrid.org/dataset/ucar.cgd.cesm2.pacific.pacemaker.html[dataset] (last access: 07 August 2023). The CESM1 Atlantic pacemaker ensemble dataset can be found here: https://www.earthsystemgrid.org/dataset/ucar.cgd.ccsm4.ATL-PACEMAKER.html. The complete description and documentation of the Pacific and Atlantic pacemaker datasets are available on the Climate Variability and Change Working Group's (CVCWG) webpage (https://www.cesm.ucar.edu/working-groups/climate/simulations/). The Earth System Model Evaluation Tool (ESMValTool Righi et al., 2020) has been used for preprocessing and calculating the CMIP6 MEM. The Tigramite package for causal discovery is available under the following public GitHub repository: https://github.com/jakobrunge/tigramite[code] (last access: 07 August 2023, Runge et al. (2023)). Details on the Multidata-PCMCI functionality can also be found on Tigramite's GitHub repository under: https://github.com/jakobrunge/tigramite/blob/master/tutorials/dataset_challenges/tigramite_tutorial_multiple_datasets.ipynb (last access: 21 Dec 2023). The code used to produce the figures for this paper is accessible at the time of publication of the paper in the following GitHub repository: xxx, last access: xxxxxx, (Karmouche, 2023).

Author contributions. SK lead the study, the writing of the manuscript, and performed all the analysis. All co-authors contributed to the concept of the study, to the interpretation of the results, and to the writing of the manuscript

Competing interests. The authors declare no competing interests.

Acknowledgements. We would like to thank two anonymous reviewers for their valuable suggestions and comments. This study was funded by the European Research Council (ERC) Synergy Grant "Understanding and modeling the Earth System with Machine Learning (USMILE)" under the Horizon 2020 research and innovation programme (Grant agreement No. 855187) and the European Union's Horizon 2020 research and innovation programme under Grant Agreement 101003536 (ESM2025—Earth System Models for the Future) as well as through the project "European Eddy-Rich ESMs" (EERIE) funded from the European Union's Horizon Europe research and innovation programme under Grant Agreement No. 101081383, the UK Research and Innovation (UKRI) under the UK government's Horizon Europe funding guarantee (grant number 10040510), and the Swiss State Secretariat for Education, Research and Innovation (SERI) under contract #22.00366. EG is supported by Central Research Development Fund at the University of Bremen, Funding No: ZF04A/2023/FB1/Galytska Evgenia. We acknowledge the World Climate Research Programme's (WCRP's) Working Group on Coupled Modelling (WGCM), and we thank the CMIP-participating climate-modeling groups for producing and making available their model output. We also thank the CVCWG for publicly publishing their ~~CESM2~~ CESM pacemaker simulations. This work used resources of the Deutsches Klimarechenzentrum (DKRZ) granted by its Scientific Steering Committee (WLA) under project no. bd1083. We also acknowledge the use of AI tools for tasks including formatting, spell-checking, and the automated generation of references in the Bibtex format.

References

Allen, R. J., Norris, J. R., and Kovilakam, M.: Influence of anthropogenic aerosols and the Pacific Decadal Oscillation on tropical belt width, Nature Geoscience, 7, 270–274, https://doi.org/10.1038/ngeo2091, 2014.

An, X., Wu, B., Zhou, T., and Liu, B.: Atlantic Multidecadal Oscillation Drives Interdecadal Pacific Variability via Tropical Atmospheric Bridge, Journal of Climate, 34, 5543–5553, https://doi.org/10.1175/jcli-d-20-0983.1, 2021.

Barnett, T. P.: Variations in Near-Global Sea Level Pressure, Journal of the Atmospheric Sciences, 42, 478–501, https://doi.org/10.1175/1520-0469(1985)042<0478:vingsl>2.0.co;2, 1985.

Bellucci, A., Mariotti, A., and Gualdi, S.: The Role of Forcings in the Twentieth-Century North Atlantic Multidecadal Variability: The 1940–75 North Atlantic Cooling Case Study, Journal of Climate, 30, 7317–7337, https://doi.org/10.1175/jcli-d-16-0301.1, 2017.

Bjerknes, J.: A possible response of the atmospheric Hadley circulation to equatorial anomalies of ocean temperature, Tellus, 18, 820–829, https://doi.org/10.1111/j.2153-3490.1966.tb00303.x, 1966.

BJERKNES, J.: ATMOSPHERIC TELECONNECTIONS FROM THE EQUATORIAL PACIFIC1, Monthly Weather Review, 97, 163–172, https://doi.org/10.1175/1520-0493(1969)097<0163:atftep>2.3.co;2, 1969.

Booth, B. B. B., Dunstone, N. J., Halloran, P. R., Andrews, T., and Bellouin, N.: Aerosols implicated as a prime driver of twentieth-century North Atlantic climate variability, Nature, 484, 228–232, https://doi.org/10.1038/nature10946, 2012.

Borchert, L. F., Koul, V., Menary, M. B., Befort, D. J., Swingedouw, D., Sgubin, G., and Mignot, J.: Skillful decadal prediction of unforced southern European summer temperature variations, Environ. Res. Lett., 16, 104 017, https://doi.org/10.1088/1748-9326/ac20f5, 2021.

Brönnimann, S.: Impact of El Niño–Southern Oscillation on European climate, Reviews of Geophysics, 45, https://doi.org/10.1029/2006rg000199, 2007.

Brönnimann, S., Xoplaki, E., Casty, C., Pauling, A., and Luterbacher, J.: ENSO influence on Europe during the last centuries, Climate Dynamics, 28, 181–197, https://doi.org/10.1007/s00382-006-0175-z, 2006.

Capotondi, A., Deser, C., Phillips, A. S., Okumura, Y., and Larson, S. M.: ENSO and Pacific Decadal Variability in the Community Earth System Model Version 2, Journal of Advances in Modeling Earth Systems, 12, https://doi.org/10.1029/2019ms002022, 2020.

Casselman, J. W., Taschetto, A. S., and Domeisen, D. I.: Non-linearity in the pathway of El Niño-Southern Oscillation to the tropical North Atlantic, Journal of Climate, p. 1–54, https://doi.org/10.1175/jcli-d-20-0952.1, 2021.

Cassou, C. and Terray, L.: Oceanic Forcing of the Wintertime Low-Frequency Atmospheric Variability in the North Atlantic European Sector: A Study with the ARPEGE Model, Journal of Climate, 14, 4266–4291, https://doi.org/10.1175/1520-0442(2001)014<4266:ofotwl>2.0.co;2, 2001.

Chang, P., Fang, Y., Saravanan, R., Ji, L., and Seidel, H.: The cause of the fragile relationship between the Pacific El Niño and the Atlantic Niño, Nature, 443, 324–328, https://doi.org/10.1038/nature05053, 2006.

Chen, H.-C., Jin, F.-F., Zhao, S., Wittenberg, A. T., and Xie, S.: ENSO Dynamics in the E3SM-1-0, CESM2, and GFDL-CM4 Climate Models, Journal of Climate, p. 1–59, https://doi.org/10.1175/jcli-d-21-0355.1, 2021.

Chiang, J. C. H. and Vimont, D. J.: Analogous Pacific and Atlantic Meridional Modes of Tropical Atmosphere–Ocean Variability*, Journal of Climate, 17, 4143–4158, https://doi.org/10.1175/jcli4953.1, 2004.

Chung, E.-S., Timmermann, A., Soden, B. J., Ha, K.-J., Shi, L., and John, V. O.: Reconciling opposing Walker circulation trends in observations and model projections, Nature Climate Change, 9, 405–412, https://doi.org/10.1038/s41558-019-0446-4, 2019.

Chylek, P., Folland, C., Klett, J. D., and Dubey, M. K.: CMIP5 Climate Models Overestimate Cooling by Volcanic Aerosols, Geophysical Research Letters, 47, https://doi.org/10.1029/2020gl087047, 2020.

Copernicus Climate Change Service: ERA5 monthly averaged data on single levels from 1979 to present, https://doi.org/10.24381/CDS.F17050D7, 2019.

Copernicus Climate Change Service: ORAS5 global ocean reanalysis monthly data from 1958 to present, https://doi.org/10.24381/CDS.67E8EEB7, 2021.

Czaja, A., van der Vaart, P., and Marshall, J.: A Diagnostic Study of the Role of Remote Forcing in Tropical Atlantic Variability, Journal of Climate, 15, 3280–3290, https://doi.org/10.1175/1520-0442(2002)015<3280:adsotr>2.0.co;2, 2002.

Danabasoglu, G., Lamarque, J., Bacmeister, J., Bailey, D. A., DuVivier, A. K., Edwards, J., Emmons, L. K., Fasullo, J., Garcia, R., Gettelman, A., Hannay, C., Holland, M. M., Large, W. G., Lauritzen, P. H., Lawrence, D. M., Lenaerts, J. T. M., Lindsay, K., Lipscomb, W. H., Mills, M. J., Neale, R., Oleson, K. W., Otto-Bliesner, B., Phillips, A. S., Sacks, W., Tilmes, S., van Kampenhout, L., Vertenstein, M., Bertini, A., Dennis, J., Deser, C., Fischer, C., Fox-Kemper, B., Kay, J. E., Kinnison, D., Kushner, P. J., Larson, V. E., Long, M. C., Mickelson, S., Moore, J. K., Nienhouse, E., Polvani, L., Rasch, P. J., and Strand, W. G.: The Community Earth System Model Version 2 (CESM2), Journal of Advances in Modeling Earth Systems, 12, https://doi.org/10.1029/2019ms001916, 2020.

Debeire, K., Runge, J., Gerhardus, A., and Eyring, V.: Bootstrap aggregation and confidence measures to improve time series causal discovery, https://doi.org/10.48550/ARXIV.2306.08946, 2023.

Deser, C.: "Certain Uncertainty: The Role of Internal Climate Variability in Projections of Regional Climate Change and Risk Management", Earth's Future, 8, https://doi.org/10.1029/2020ef001854, 2020.

Deser, C. and Phillips, A. S.: A range of outcomes: the combined effects of internal variability and anthropogenic forcing on regional climate trends over Europe, Nonlinear Processes in Geophysics, 30, 63–84, https://doi.org/10.5194/npg-30-63-2023, 2023.

Deser, C., Phillips, A., Bourdette, V., and Teng, H.: Uncertainty in climate change projections: the role of internal variability, Climate Dynamics, 38, 527–546, https://doi.org/10.1007/s00382-010-0977-x, 2010.

DiNezio, P. N., Vecchi, G. A., and Clement, A. C.: Detectability of Changes in the Walker Circulation in Response to Global Warming*, Journal of Climate, 26, 4038–4048, https://doi.org/10.1175/jcli-d-12-00531.1, 2013.

Dong, L. and McPhaden, M. J.: The role of external forcing and internal variability in regulating global mean surface temperatures on decadal timescales, Environmental Research Letters, 12, 034 011, https://doi.org/10.1088/1748-9326/aa5dd8, 2017.

Dong, L., Zhou, T., and Chen, X.: Changes of Pacific decadal variability in the twentieth century driven by internal variability, greenhouse gases, and aerosols, Geophysical Research Letters, 41, 8570–8577, https://doi.org/10.1002/2014gl062269, 2014.

Enfield, D. B. and Mayer, D. A.: Tropical Atlantic sea surface temperature variability and its relation to El Niño-Southern Oscillation, Journal of Geophysical Research, 102, 929–945, https://doi.org/https://doi.org/10.1029/96JC03296, 1997.

Enfield, D. B., Mestas-Nuñez, A. M., Mayer, D. A., and Cid-Serrano, L.: How ubiquitous is the dipole relationship in tropical Atlantic sea surface temperatures?, Journal of Geophysical Research: Oceans, 104, 7841–7848, https://doi.org/10.1029/1998jc900109, 1999.

Eyring, V., Bony, S., Meehl, G. A., Senior, C. A., Stevens, B., Stouffer, R. J., and Taylor, K. E.: Overview of the Coupled Model Intercomparison Project Phase 6 (CMIP6) experimental design and organization, Geoscientific Model Development, 9, 1937–1958, https://doi.org/10.5194/gmd-9-1937-2016, 2016.

Eyring, V., Cox, P. M., Flato, G. M., Gleckler, P. J., Abramowitz, G., Caldwell, P., Collins, W. D., Gier, B. K., Hall, A. D., Hoffman, F. M., Hurtt, G. C., Jahn, A., Jones, C. D., Klein, S. A., Krasting, J. P., Kwiatkowski, L., Lorenz, R., Maloney, E., Meehl, G. A., Pendergrass, A. G., Pincus, R., Ruane, A. C., Russell, J. L., Sanderson, B. M., Santer, B. D., Sherwood, S. C., Simpson, I. R., Stouffer, R. J., and

Williamson, M. S.: Taking climate model evaluation to the next level, Nature Climate Change, 9, 102–110, https://doi.org/10.1038/s41558-018-0355-y, 2019.

Eyring, V., Gillett, N. P., Achuta Rao, K. M., Barimalala, R., Barreiro Parrillo, M., Bellouin, N., Cassou, C., Durack, P. J., Kosaka, Y., McGregor, S., Min, S.-K., Morgenstern, O., and Sun, Y.: Human Influence on the Climate System, pp. 423–552, Cambridge University Press, Cambridge, United Kingdom and New York, NY, USA, https://doi.org/10.1017/9781009157896.005, 2021.

Fasullo, J. T., Phillips, A. S., and Deser, C.: Evaluation of Leading Modes of Climate Variability in the CMIP Archives, Journal of Climate, 33, 5527–5545, https://doi.org/10.1175/jcli-d-19-1024.1, 2020.

Fyfe, J. C., Kharin, V. V., Santer, B. D., Cole, J. N. S., and Gillett, N. P.: Significant impact of forcing uncertainty in a large ensemble of climate model simulations, Proceedings of the National Academy of Sciences, 118, https://doi.org/10.1073/pnas.2016549118, 2021.

Galytska, E., Weigel, K., Handorf, D., Jaiser, R., Köhler, R. H., Runge, J., and Eyring, V.: Causal model evaluation of Arctic-midlatitude teleconnections in CMIP6, https://doi.org/10.1002/essoar.10512569.1, 2022.

García-Serrano, J., Cassou, C., Douville, H., Giannini, A., and Doblas-Reyes, F. J.: Revisiting the ENSO Teleconnection to the Tropical North Atlantic, Journal of Climate, 30, 6945–6957, https://doi.org/10.1175/jcli-d-16-0641.1, 2017a.

García-Serrano, J., Cassou, C., Douville, H., Giannini, A., and Doblas-Reyes, F. J.: Revisiting the ENSO Teleconnection to the Tropical North Atlantic, Journal of Climate, 30, 6945–6957, https://doi.org/10.1175/jcli-d-16-0641.1, 2017b.

Gerhardus, A. and Runge, J.: High-recall causal discovery for autocorrelated time series with latent confounders, https://doi.org/10.48550/ARXIV.2007.01884, 2020.

Gill, A. E.: Some simple solutions for heat-induced tropical circulation, Quarterly Journal of the Royal Meteorological Society, 106, 447–462, https://doi.org/10.1002/qj.49710644905, 1980.

Ham, Y., Kug, J., and Park, J.: Two distinct roles of Atlantic SSTs in ENSO variability: North Tropical Atlantic SST and Atlantic Niño, Geophysical Research Letters, 40, 4012–4017, https://doi.org/10.1002/grl.50729, 2013a.

Ham, Y.-G., Kug, J.-S., Park, J.-Y., and Jin, F.-F.: Sea surface temperature in the north tropical Atlantic as a trigger for El Niño/Southern Oscillation events, Nature Geoscience, 6, 112–116, https://doi.org/10.1038/ngeo1686, 2013b.

Haustein, K., Otto, F. E. L., Venema, V., Jacobs, P., Cowtan, K., Hausfather, Z., Way, R. G., White, B., Subramanian, A., and Schurer, A. P.: A Limited Role for Unforced Internal Variability in Twentieth-Century Warming, Journal of Climate, 32, 4893–4917, https://doi.org/10.1175/jcli-d-18-0555.1, 2019.

He, C., Clement, A., Kramer, S., Cane, M., Klavans, J., Fenske, T., and Murphy, L.: Recent Atlantic multidecadal variability and its impacts are driven by external forcings, https://doi.org/10.21203/rs.3.rs-2561784/v1, 2023.

Honda, M., Nakamura, H., Ukita, J., Kousaka, I., and Takeuchi, K.: Interannual Seesaw between the Aleutian and Icelandic Lows. Part I: Seasonal Dependence and Life Cycle, Journal of Climate, 14, 1029–1042, https://doi.org/10.1175/1520-0442(2001)014<1029:isbtaa>2.0.co;2, 2001.

Hoskins, B. J. and Karoly, D. J.: The Steady Linear Response of a Spherical Atmosphere to Thermal and Orographic Forcing, Journal of the Atmospheric Sciences, 38, 1179–1196, https://doi.org/10.1175/1520-0469(1981)038<1179:tslroa>2.0.co;2, 1981.

Hurrell, J. W. and Deser, C.: North Atlantic climate variability: The role of the North Atlantic Oscillation, Journal of Marine Systems, 78, 28–41, https://doi.org/10.1016/j.jmarsys.2008.11.026, 2009.

IPCC: Climate Change 2013: The Physical Science Basis. Contribution of Working Group I to the Fifth Assessment Report of the Intergovernmental Panel on Climate Change, Cambridge University Press, Cambridge, 2013.

Jiang, L. and Li, T.: Relative roles of El Niño-induced extratropical and tropical forcing in generating Tropical North Atlantic (TNA) SST anomaly, Climate Dynamics, 53, 3791–3804, https://doi.org/10.1007/s00382-019-04748-7, 2019.

Kalnay, E., Kanamitsu, M., Kistler, R., Collins, W., Deaven, D., Gandin, L., Iredell, M., Saha, S., White, G., Woollen, J., Zhu, Y., Leetmaa, A., Reynolds, R., Chelliah, M., Ebisuzaki, W., Higgins, W., Janowiak, J., Mo, K. C., Ropelewski, C., Wang, J., Jenne, R., and Joseph, D.: The NCEP/NCAR 40-Year Reanalysis Project, Bulletin of the American Meteorological Society, 77, 437–471, https://doi.org/10.1175/1520-0477(1996)077<0437:tnyrp>2.0.co;2, 1996.

Karmouche, S., Galytska, E., Runge, J., Meehl, G. A., Phillips, A. S., Weigel, K., and Eyring, V.: Regime-oriented causal model evaluation of Atlantic–Pacific teleconnections in CMIP6, Earth System Dynamics, 14, 309–344, https://doi.org/10.5194/esd-14-309-2023, 2023.

Karoly, D. J.: Rossby wave propagation in a barotropic atmosphere, Dynamics of Atmospheres and Oceans, 7, 111–125, https://doi.org/10.1016/0377-0265(83)90013-1, 1983.

Kaufmann, R. K., Kauppi, H., Mann, M. L., and Stock, J. H.: Reconciling anthropogenic climate change with observed temperature 1998–2008, Proceedings of the National Academy of Sciences, 108, 11 790–11 793, https://doi.org/10.1073/pnas.1102467108, 2011.

Keenlyside, N. S., Ding, H., and Latif, M.: Potential of equatorial Atlantic variability to enhance El Niño prediction, Geophysical Research Letters, 40, 2278–2283, https://doi.org/10.1002/grl.50362, 2013.

Klavans, J. M., Cane, M. A., Clement, A. C., and Murphy, L. N.: NAO predictability from external forcing in the late 20th century, npj Climate and Atmospheric Science, 4, https://doi.org/10.1038/s41612-021-00177-8, 2021.

Klavans, J. M., Clement, A. C., Cane, M. A., and Murphy, L. N.: The Evolving Role of External Forcing in North Atlantic SST Variability over the Last Millennium, Journal of Climate, 35, 2741–2754, https://doi.org/10.1175/jcli-d-21-0338.1, 2022.

Klein, S. A., Soden, B. J., and Lau, N.-C.: Remote Sea Surface Temperature Variations during ENSO: Evidence for a Tropical Atmospheric Bridge, Journal of Climate, 12, 917–932, https://doi.org/10.1175/1520-0442(1999)012<0917:rsstvd>2.0.co;2, 1999.

Kociuba, G. and Power, S. B.: Inability of CMIP5 Models to Simulate Recent Strengthening of the Walker Circulation: Implications for Projections, Journal of Climate, 28, 20–35, https://doi.org/10.1175/jcli-d-13-00752.1, 2014.

Kosaka, Y. and Xie, S.-P.: Recent global-warming hiatus tied to equatorial Pacific surface cooling, Nature, 501, 403–407, https://doi.org/10.1038/nature12534, 2013.

Kucharski, F., Kang, I.-S., Farneti, R., and Feudale, L.: Tropical Pacific response to 20th century Atlantic warming: PACIFIC RESPONSE TO ATLANTIC WARMING, Geophysical Research Letters, 38, https://doi.org/10.1029/2010gl046248, 2011.

Kucharski, F., Ikram, F., Molteni, F., Farneti, R., Kang, I.-S., No, H.-H., King, M. P., Giuliani, G., and Mogensen, K.: Atlantic forcing of Pacific decadal variability, Climate Dynamics, 46, 2337–2351, https://doi.org/10.1007/s00382-015-2705-z, 2015.

Kumar, A., Jha, B., and Wang, H.: Attribution of SST variability in global oceans and the role of ENSO, Climate Dynamics, 43, 209–220, https://doi.org/10.1007/s00382-013-1865-y, 2013.

Latif, M. and Grötzner, A.: The equatorial Atlantic oscillation and its response to ENSO, Climate Dynamics, 16, 213–218, https://doi.org/10.1007/s003820050014, 2000.

Lee, S., Enfield, D. B., and Wang, C.: Why do some El Niños have no impact on tropical North Atlantic SST?, Geophysical Research Letters, 35, https://doi.org/10.1029/2008gl034734, 2008.

Lengaigne, M., Boulanger, J., Menkes, C., Masson, S., Madec, G., and Delecluse, P.: Ocean response to the March 1997 Westerly Wind Event, Journal of Geophysical Research: Oceans, 107, https://doi.org/10.1029/2001jc000841, 2002.

Lengaigne, M., Boulanger, J.-P., Menkes, C., Madec, G., Delecluse, P., Guilyardi, E., and Slingo, J.: The March 1997 Westerly Wind Event and the Onset of the 1997/98 El Niño: Understanding the Role of the Atmospheric Response, Journal of Climate, 16, 3330–3343, https://doi.org/10.1175/1520-0442(2003)016<3330:tmwwea>2.0.co;2, 2003.

Lengaigne, M., Guilyardi, E., Boulanger, J.-P., Menkes, C., Delecluse, P., Inness, P., Cole, J., and Slingo, J.: Triggering of El Niño by westerly wind events in a coupled general circulation model, Climate Dynamics, 23, 601–620, https://doi.org/10.1007/s00382-004-0457-2, 2004.

Levine, A. F. Z., McPhaden, M. J., and Frierson, D. M. W.: The impact of the AMO on multidecadal ENSO variability, Geophysical Research Letters, 44, 3877–3886, https://doi.org/10.1002/2017gl072524, 2017.

Li, X., Xie, S.-P., Gille, S. T., and Yoo, C.: Atlantic-induced pan-tropical climate change over the past three decades, Nature Climate Change, 6, 275–279, https://doi.org/10.1038/nclimate2840, 2015.

Lian, T. and Chen, D.: The essential role of early-spring westerly wind burst in generating the centennial extreme 1997/98 El Niño, Journal of Climate, p. 1–38, https://doi.org/10.1175/jcli-d-21-0010.1, 2021.

Lin, H. and Derome, J.: Nonlinearity of the Extratropical Response to Tropical Forcing, Journal of Climate, 17, 2597–2608, https://doi.org/10.1175/1520-0442(2004)017<2597:notert>2.0.co;2, 2004.

Luo, J.-J., Sasaki, W., and Masumoto, Y.: Indian Ocean warming modulates Pacific climate change, Proceedings of the National Academy of Sciences, 109, 18 701–18 706, https://doi.org/10.1073/pnas.1210239109, 2012.

L'Heureux, M. L., Lee, S., and Lyon, B.: Recent multidecadal strengthening of the Walker circulation across the tropical Pacific, Nature Climate Change, 3, 571–576, https://doi.org/10.1038/nclimate1840, 2013.

Maher, N., McGregor, S., England, M. H., and Gupta, A. S.: Effects of volcanism on tropical variability, Geophysical Research Letters, 42, 6024–6033, https://doi.org/10.1002/2015gl064751, 2015.

Maher, N., Matei, D., Milinski, S., and Marotzke, J.: ENSO Change in Climate Projections: Forced Response or Internal Variability?, Geophysical Research Letters, 45, https://doi.org/10.1029/2018gl079764, 2018.

Mann, M. E., Steinman, B. A., and Miller, S. K.: On forced temperature changes, internal variability, and the AMO: INTERNAL VARIABILITY AND THE AMO, Geophysical Research Letters, 41, 3211–3219, https://doi.org/10.1002/2014gl059233, 2014.

Mantua, N. J., Hare, S. R., Zhang, Y., Wallace, J. M., and Francis, R. C.: A Pacific Interdecadal Climate Oscillation with Impacts on Salmon Production, Bulletin of the American Meteorological Society, 78, 1069–1079, https://doi.org/10.1175/1520-0477(1997)078<1069:apicow>2.0.co;2, 1997.

Martín-Rey, M., Rodríguez-Fonseca, B., Polo, I., and Kucharski, F.: On the Atlantic–Pacific Niños connection: a multidecadal modulated mode, Climate Dynamics, 43, 3163–3178, https://doi.org/10.1007/s00382-014-2305-3, 2014a.

Martín-Rey, M., Rodríguez-Fonseca, B., Polo, I., and Kucharski, F.: On the Atlantic–Pacific Niños connection: a multidecadal modulated mode, Climate Dynamics, 43, 3163–3178, https://doi.org/10.1007/s00382-014-2305-3, 2014b.

Masson-Delmotte, V., Zhai, P., Pirani, A., Connors, S. L., Péan, C., Berger, S., Caud, N., Chen, Y., Goldfarb, L., Gomis, M. I., Huang, M., Leitzell, K., Lonnoy, E., Matthews, J. B. R., Maycock, T. K., Waterfield, T., Yelekçi, , Yu, R., and Zhou, B.: AR6, Annex IV: Modes of Variability, p. 2153–2192, Cambridge University Press, https://doi.org/10.1017/9781009157896.018, 2023.

Matsuno, T.: Quasi-Geostrophic Motions in the Equatorial Area, Journal of the Meteorological Society of Japan. Ser. II, 44, 25–43, https://doi.org/10.2151/jmsj1965.44.1_25, 1966.

McBride, L. A., Hope, A. P., Canty, T. P., Bennett, B. F., Tribett, W. R., and Salawitch, R. J.: Comparison of CMIP6 historical climate simulations and future projected warming to an empirical model of global climate, Earth System Dynamics, 12, 545–579, https://doi.org/10.5194/esd-12-545-2021, 2021.

McGregor, S., Timmermann, A., Stuecker, M. F., England, M. H., Merrifield, M., Jin, F.-F., and Chikamoto, Y.: Recent Walker circulation strengthening and Pacific cooling amplified by Atlantic warming, Nature Climate Change, 4, 888–892, https://doi.org/10.1038/nclimate2330, 2014.

McPhaden, M. J.: Genesis and Evolution of the 1997-98 El Niño, Science, 283, 950–954, https://doi.org/10.1126/science.283.5404.950, 1999.

Meehl, G. A., Hu, A., Arblaster, J. M., Fasullo, J., and Trenberth, K. E.: Externally Forced and Internally Generated Decadal Climate Variability Associated with the Interdecadal Pacific Oscillation, Journal of Climate, 26, 7298–7310, https://doi.org/10.1175/jcli-d-12-00548.1, 2013.

Meehl, G. A., Hu, A., Santer, B. D., and Xie, S.-P.: Contribution of the Interdecadal Pacific Oscillation to twentieth-century global surface temperature trends, Nature Climate Change, 6, 1005–1008, https://doi.org/10.1038/nclimate3107, 2016.

Meehl, G. A., Chung, C. T. Y., Arblaster, J. M., Holland, M. M., and Bitz, C. M.: Tropical Decadal Variability and the Rate of Arctic Sea Ice Decrease, Geophysical Research Letters, 45, https://doi.org/10.1029/2018gl079989, 2018.

Meehl, G. A., Hu, A., Castruccio, F., England, M. H., Bates, S. C., Danabasoglu, G., McGregor, S., Arblaster, J. M., Xie, S.-P., and Rosenbloom, N.: Atlantic and Pacific tropics connected by mutually interactive decadal-timescale processes, Nature Geoscience, 14, 36–42, https://doi.org/10.1038/s41561-020-00669-x, 2020.

Menary, M. B., Robson, J., Allan, R. P., Booth, B. B. B., Cassou, C., Gastineau, G., Gregory, J., Hodson, D., Jones, C., Mignot, J., Ringer, M., Sutton, R., Wilcox, L., and Zhang, R.: Aerosol-Forced AMOC Changes in CMIP6 Historical Simulations, Geophysical Research Letters, 47, https://doi.org/10.1029/2020gl088166, 2020.

Milinski, S., Maher, N., and Olonscheck, D.: How large does a large ensemble need to be?, Earth System Dynamics, 11, 885–901, https://doi.org/10.5194/esd-11-885-2020, 2020.

Murphy, L. N., Bellomo, K., Cane, M., and Clement, A.: The role of historical forcings in simulating the observed Atlantic multidecadal oscillation, Geophysical Research Letters, 44, 2472–2480, https://doi.org/10.1002/2016gl071337, 2017.

Murtugudde, R. G., Ballabrera-Poy, J., Beauchamp, J., and Busalacchi, A. J.: Relationship between zonal and meridional modes in the tropical Atlantic, Geophysical Research Letters, 28, 4463–4466, https://doi.org/10.1029/2001gl013407, 2001.

Neelin, J. D., Battisti, D. S., Hirst, A. C., Jin, F., Wakata, Y., Yamagata, T., and Zebiak, S. E.: ENSO theory, Journal of Geophysical Research: Oceans, 103, 14 261–14 290, https://doi.org/10.1029/97jc03424, 1998.

Newman, M., Alexander, M. A., Ault, T. R., Cobb, K. M., Deser, C., Di Lorenzo, E., Mantua, N. J., Miller, A. J., Minobe, S., Nakamura, H., Schneider, N., Vimont, D. J., Phillips, A. S., Scott, J. D., and Smith, C. A.: The Pacific Decadal Oscillation, Revisited, Journal of Climate, 29, 4399–4427, https://doi.org/10.1175/jcli-d-15-0508.1, 2016.

O'Brien, J. P. and Deser, C.: Quantifying and Understanding Forced Changes to Unforced Modes of Atmospheric Circulation Variability over the North Pacific in a Coupled Model Large Ensemble, Journal of Climate, 36, 19–37, https://doi.org/10.1175/jcli-d-22-0101.1, 2023.

Park, J.-H. and Li, T.: Interdecadal modulation of El Niño–tropical North Atlantic teleconnection by the Atlantic multi-decadal oscillation, Climate Dynamics, 52, 5345–5360, https://doi.org/10.1007/s00382-018-4452-4, 2018.

Park, J.-H., Li, T., Yeh, S.-W., and Kim, H.: Effect of recent Atlantic warming in strengthening Atlantic–Pacific teleconnection on interannual timescale via enhanced connection with the pacific meridional mode, Climate Dynamics, 53, 371–387, https://doi.org/10.1007/s00382-018-4591-7, 2019.

Park, J.-H., Sung, M.-K., Yang, Y.-M., Zhao, J., An, S.-I., and Kug, J.-S.: Role of the climatological intertropical convergence zone in the seasonal footprinting mechanism of the El Niño-Southern Oscillation, Journal of Climate, p. 1–43, https://doi.org/10.1175/jcli-d-20-0809.1, 2021.

Park, J.-H., Kug, J.-S., Yang, Y.-M., Oh, H., Zhao, J., and Wu, Y.: Role of the Climatological North Pacific High in the North Tropical Atlantic–ENSO Connection, Journal of Climate, 35, 3215–3226, https://doi.org/10.1175/jcli-d-21-0933.1, 2022.

Park, J.-H., Kug, J.-S., Yang, Y.-M., Sung, M.-K., Kim, S., Kim, H.-J., Park, H.-J., and An, S.-I.: Distinct decadal modulation of Atlantic-Niño influence on ENSO, npj Climate and Atmospheric Science, 6, https://doi.org/10.1038/s41612-023-00429-9, 2023a.

Park, J.-H., Yeh, S.-W., Kug, J.-S., Yang, Y.-M., Jo, H.-S., Kim, H.-J., and An, S.-I.: Two regimes of inter-basin interactions between the Atlantic and Pacific Oceans on interannual timescales, npj Climate and Atmospheric Science, 6, https://doi.org/10.1038/s41612-023-00332-3, 2023b.

Phillips, A., Deser, C., Fasullo, J., Schneider, D. P., and Simpson, I. R.: Assessing Climate Variability and Change in Model Large Ensembles: A User's Guide to the "Climate Variability Diagnostics Package for Large Ensembles", https://doi.org/10.5065/H7C7-F961, 2020.

Pinto, J. G., Reyers, M., and Ulbrich, U.: The variable link between PNA and NAO in observations and in multi-century CGCM simulations, Climate Dynamics, 36, 337–354, https://doi.org/10.1007/s00382-010-0770-x, 2010.

Polyakov, I. V. and Johnson, M. A.: Arctic decadal and interdecadal variability, Geophysical Research Letters, 27, 4097–4100, https://doi.org/10.1029/2000gl011909, 2000.

Power, S. B. and Kociuba, G.: What Caused the Observed Twentieth-Century Weakening of the Walker Circulation?, Journal of Climate, 24, 6501–6514, https://doi.org/10.1175/2011jcli4101.1, 2011.

Rajagopalan, B., Kushnir, Y., and Tourre, Y. M.: Observed decadal midlatitude and tropical Atlantic climate variability, Geophysical Research Letters, 25, 3967–3970, https://doi.org/10.1029/1998gl900065, 1998.

Rayner, N. A., Parker, D. E., Horton, E. B., Folland, C. K., Alexander, L. V., Rowell, D. P., Kent, E. C., and Kaplan, A.: Global analyses of sea surface temperature, sea ice, and night marine air temperature since the late nineteenth century, Journal of Geophysical Research: Atmospheres, 108, https://doi.org/10.1029/2002jd002670, 2003.

Righi, M., Andela, B., Eyring, V., Lauer, A., Predoi, V., Schlund, M., Vegas-Regidor, J., Bock, L., Brötz, B., de Mora, L., Diblen, F., Dreyer, L., Drost, N., Earnshaw, P., Hassler, B., Koldunov, N., Little, B., Loosveldt Tomas, S., and Zimmermann, K.: Earth System Model Evaluation Tool (ESMValTool) v2.0 – technical overview, Geoscientific Model Development, 13, 1179–1199, https://doi.org/10.5194/gmd-13-1179-2020, 2020.

Runge, J.: Discovering contemporaneous and lagged causal relations in autocorrelated nonlinear time series datasets, arXiv, https://doi.org/10.48550/ARXIV.2003.03685, 2020.

Runge, J., Petoukhov, V., Donges, J. F., Hlinka, J., Jajcay, N., Vejmelka, M., Hartman, D., Marwan, N., Paluš, M., and Kurths, J.: Identifying causal gateways and mediators in complex spatio-temporal systems, Nature Communications, 6, https://doi.org/10.1038/ncomms9502, 2015.

Runge, J., Nowack, P., Kretschmer, M., Flaxman, S., and Sejdinovic, D.: Detecting and quantifying causal associations in large nonlinear time series datasets, Science Advances, 5, https://doi.org/10.1126/sciadv.aau4996, 2019.

Runge, J., Gerhardus, A., Varando, G., Eyring, V., and Camps-Valls, G.: Causal inference for time series, Nature Reviews Earth amp; Environment, 4, 487–505, https://doi.org/10.1038/s43017-023-00431-y, 2023.

Ruprich-Robert, Y., Msadek, R., Castruccio, F., Yeager, S., Delworth, T., and Danabasoglu, G.: Assessing the Climate Impacts of the Observed Atlantic Multidecadal Variability Using the GFDL CM2.1 and NCAR CESM1 Global Coupled Models, Journal of Climate, 30, 2785–2810, https://doi.org/10.1175/jcli-d-16-0127.1, 2017.

Saravanan, R. and Chang, P.: Interaction between Tropical Atlantic Variability and El Niño–Southern Oscillation, Journal of Climate, 13, 2177–2194, https://doi.org/10.1175/1520-0442(2000)013<2177:ibtava>2.0.co;2, 2000.

Sato, Y., Goto, D., Michibata, T., Suzuki, K., Takemura, T., Tomita, H., and Nakajima, T.: Aerosol effects on cloud water amounts were successfully simulated by a global cloud-system resolving model, Nature Communications, 9, https://doi.org/10.1038/s41467-018-03379-6, 2018.

Scaife, A. A., Arribas, A., Blockley, E., Brookshaw, A., Clark, R. T., Dunstone, N., Eade, R., Fereday, D., Folland, C. K., Gordon, M., Hermanson, L., Knight, J. R., Lea, D. J., MacLachlan, C., Maidens, A., Martin, M., Peterson, A. K., Smith, D., Vellinga, M., Wallace, E., Waters, J., and Williams, A.: Skillful long-range prediction of European and North American winters, Geophysical Research Letters, 41, 2514–2519, https://doi.org/10.1002/2014gl059637, 2014.

Schlund, M., Lauer, A., Gentine, P., Sherwood, S. C., and Eyring, V.: Emergent constraints on equilibrium climate sensitivity in CMIP5: do they hold for CMIP6?, Earth System Dynamics, 11, 1233–1258, https://doi.org/10.5194/esd-11-1233-2020, 2020.

Smirnov, D. A. and Bezruchko, B. P.: Spurious causalities due to low temporal resolution: Towards detection of bidirectional coupling from time series, EPL (Europhysics Letters), 100, 10 005, https://doi.org/10.1209/0295-5075/100/10005, 2012.

Smith, C. J. and Forster, P. M.: Suppressed Late-20th Century Warming in CMIP6 Models Explained by Forcing and Feedbacks, Geophysical Research Letters, 48, https://doi.org/10.1029/2021gl094948, 2021.

Smith, C. J., Harris, G. R., Palmer, M. D., Bellouin, N., Collins, W., Myhre, G., Schulz, M., Golaz, J., Ringer, M., Storelvmo, T., and Forster, P. M.: Energy Budget Constraints on the Time History of Aerosol Forcing and Climate Sensitivity, Journal of Geophysical Research: Atmospheres, 126, https://doi.org/10.1029/2020jd033622, 2021.

Smith, D. M., Booth, B. B. B., Dunstone, N. J., Eade, R., Hermanson, L., Jones, G. S., Scaife, A. A., Sheen, K. L., and Thompson, V.: Role of volcanic and anthropogenic aerosols in the recent global surface warming slowdown, Nature Climate Change, 6, 936–940, https://doi.org/10.1038/nclimate3058, 2016.

Smith, D. M., Eade, R., Scaife, A. A., Caron, L.-P., Danabasoglu, G., DelSole, T. M., Delworth, T., Doblas-Reyes, F. J., Dunstone, N. J., Hermanson, L., Kharin, V., Kimoto, M., Merryfield, W. J., Mochizuki, T., Müller, W. A., Pohlmann, H., Yeager, S., and Yang, X.: Robust skill of decadal climate predictions, npj Climate and Atmospheric Science, 2, 13, https://doi.org/https://doi.org/10.1038/s41612-019-0071-y, 2019.

Smith, D. M., Gillett, N. P., Simpson, I. R., Athanasiadis, P. J., Baehr, J., Bethke, I., Bilge, T. A., Bonnet, R., Boucher, O., Findell, K. L., Gastineau, G., Gualdi, S., Hermanson, L., Leung, L. R., Mignot, J., Müller, W. A., Osprey, S., Otterå, O. H., Persad, G. G., Scaife, A. A., Schmidt, G. A., Shiogama, H., Sutton, R. T., Swingedouw, D., Yang, S., Zhou, T., and Ziehn, T.: Attribution of multi-annual to decadal changes in the climate system: The Large Ensemble Single Forcing Model Intercomparison Project (LESFMIP), Frontiers in Climate, 4, https://doi.org/10.3389/fclim.2022.955414, 2022.

Song, J., Li, C., Zhou, W., and Pan, J.: The linkage between the Pacific-North American teleconnection pattern and the North Atlantic Oscillation, Advances in Atmospheric Sciences, 26, 229–239, https://doi.org/10.1007/s00376-009-0229-3, 2009.

Soulard, N. and Lin, H.: The spring relationship between the Pacific-North American pattern and the North Atlantic Oscillation, Climate Dynamics, 48, 619–629, https://doi.org/10.1007/s00382-016-3098-3, 2016.

Sutton, R. T., Jewson, S. P., and Rowell, D. P.: The Elements of Climate Variability in the Tropical Atlantic Region, Journal of Climate, 13, 3261–3284, https://doi.org/10.1175/1520-0442(2000)013<3261:teocvi>2.0.co;2, 2000.

Taschetto, A. S., Rodrigues, R. R., Meehl, G. A., McGregor, S., and England, M. H.: How sensitive are the Pacific–tropical North Atlantic teleconnections to the position and intensity of El Niño-related warming?, Climate Dynamics, 46, 1841–1860, https://doi.org/10.1007/s00382-015-2679-x, 2015.

Tebaldi, C., Dorheim, K., Wehner, M., and Leung, R.: Extreme metrics from large ensembles: investigating the effects of ensemble size on their estimates, Earth System Dynamics, 12, 1427–1501, https://doi.org/10.5194/esd-12-1427-2021, 2021.

Tokarska, K. B., Hegerl, G. C., Schurer, A. P., Forster, P. M., and Marvel, K.: Observational constraints on the effective climate sensitivity from the historical period, Environmental Research Letters, 15, 034 043, https://doi.org/10.1088/1748-9326/ab738f, 2020a.

Tokarska, K. B., Stolpe, M. B., Sippel, S., Fischer, E. M., Smith, C. J., Lehner, F., and Knutti, R.: Past warming trend constrains future warming in CMIP6 models, Science Advances, 6, https://doi.org/10.1126/sciadv.aaz9549, 2020b.

Trenberth, K. E.: The Definition of El Niño, Bulletin of the American Meteorological Society, 78, 2771–2777, https://doi.org/10.1175/1520-0477(1997)078<2771:tdoeno>2.0.co;2, 1997.

Trenberth, K. E. and Shea, D. J.: Atlantic hurricanes and natural variability in 2005, Geophysical Research Letters, 33, https://doi.org/10.1029/2006gl026894, 2006.

Vecchi, G. A. and Soden, B. J.: Global Warming and the Weakening of the Tropical Circulation, Journal of Climate, 20, 4316–4340, https://doi.org/10.1175/jcli4258.1, 2007.

Visbeck, M., Chassignet, E. P., Curry, R. G., Delworth, T. L., Dickson, R. R., and Krahmann, G.: The ocean's response to North Atlantic Oscillation variability, p. 113–145, https://doi.org/10.1029/134gm06, 2003.

Wallace, J. M. and Gutzler, D. S.: Teleconnections in the Geopotential Height Field during the Northern Hemisphere Winter, Monthly Weather Review, 109, 784–812, https://doi.org/10.1175/1520-0493(1981)109<0784:titghf>2.0.co;2, 1981.

Wang, C.: Atlantic Climate Variability and Its Associated Atmospheric Circulation Cells, Journal of Climate, 15, 1516–1536, https://doi.org/10.1175/1520-0442(2002)015<1516:acvaia>2.0.co;2, 2002.

Wang, C.: A review of ENSO theories, National Science Review, 5, 813–825, https://doi.org/10.1093/nsr/nwy104, 2018.

Wang, C.: Three-ocean interactions and climate variability: a review and perspective, Climate Dynamics, 53, 5119–5136, https://doi.org/10.1007/s00382-019-04930-x, 2019.

Wang, J., Yang, B., Ljungqvist, F. C., Luterbacher, J., Osborn, T. J., Briffa, K. R., and Zorita, E.: Internal and external forcing of multidecadal Atlantic climate variability over the past 1, 200 years, Nature Geoscience, 10, 512–517, https://doi.org/10.1038/ngeo2962, 2017a.

Wang, L., Yu, J.-Y., and Paek, H.: Enhanced biennial variability in the Pacific due to Atlantic capacitor effect, Nature Communications, 8, https://doi.org/10.1038/ncomms14887, 2017b.

Watanabe, M. and Tatebe, H.: Reconciling roles of sulphate aerosol forcing and internal variability in Atlantic multidecadal climate changes, Climate Dynamics, 53, 4651–4665, https://doi.org/10.1007/s00382-019-04811-3, 2019.

Wei, M., Shu, Q., Song, Z., Song, Y., Yang, X., Guo, Y., Li, X., and Qiao, F.: Could CMIP6 climate models reproduce the early-2000s global warming slowdown?, Science China Earth Sciences, 64, 853–865, https://doi.org/10.1007/s11430-020-9740-3, 2021.

Wu, M., Zhou, T., Li, C., Li, H., Chen, X., Wu, B., Zhang, W., and Zhang, L.: A very likely weakening of Pacific Walker Circulation in constrained near-future projections, Nature Communications, 12, https://doi.org/10.1038/s41467-021-26693-y, 2021.

Yang, D., Arblaster, J. M., Meehl, G. A., England, M. H., Lim, E.-P., Bates, S., and Rosenbloom, N.: Role of Tropical Variability in Driving Decadal Shifts in the Southern Hemisphere Summertime Eddy-Driven Jet, Journal of Climate, 33, 5445–5463, https://doi.org/10.1175/jcli-d-19-0604.1, 2020.

Yang, Y., Wu, L., Guo, Y., Gan, B., Cai, W., Huang, G., Li, X., Geng, T., Jing, Z., Li, S., Liang, X., and Xie, S.-P.: Greenhouse warming intensifies north tropical Atlantic climate variability, Science Advances, 7, https://doi.org/10.1126/sciadv.abg9690, 2021.

Yang, Y.-M., An, S.-I., Wang, B., and Park, J. H.: A global-scale multidecadal variability driven by Atlantic multidecadal oscillation, National Science Review, 7, 1190–1197, https://doi.org/10.1093/nsr/nwz216, 2019.

Zebiak, S. E.: Air–Sea Interaction in the Equatorial Atlantic Region, Journal of Climate, 6, 1567–1586, https://doi.org/10.1175/1520-0442(1993)006<1567:aiitea>2.0.co;2, 1993.

Zhang, R., Sutton, R., Danabasoglu, G., Kwon, Y.-O., Marsh, R., Yeager, S. G., Amrhein, D. E., and Little, C. M.: A review of the role of the Atlantic Meridional Overturning Circulation in Atlantic Multidecadal Variability and associated climate impacts, Rev. Geophys., 57, 316–375, https://doi.org/10.1029/2019RG000644, 2019.

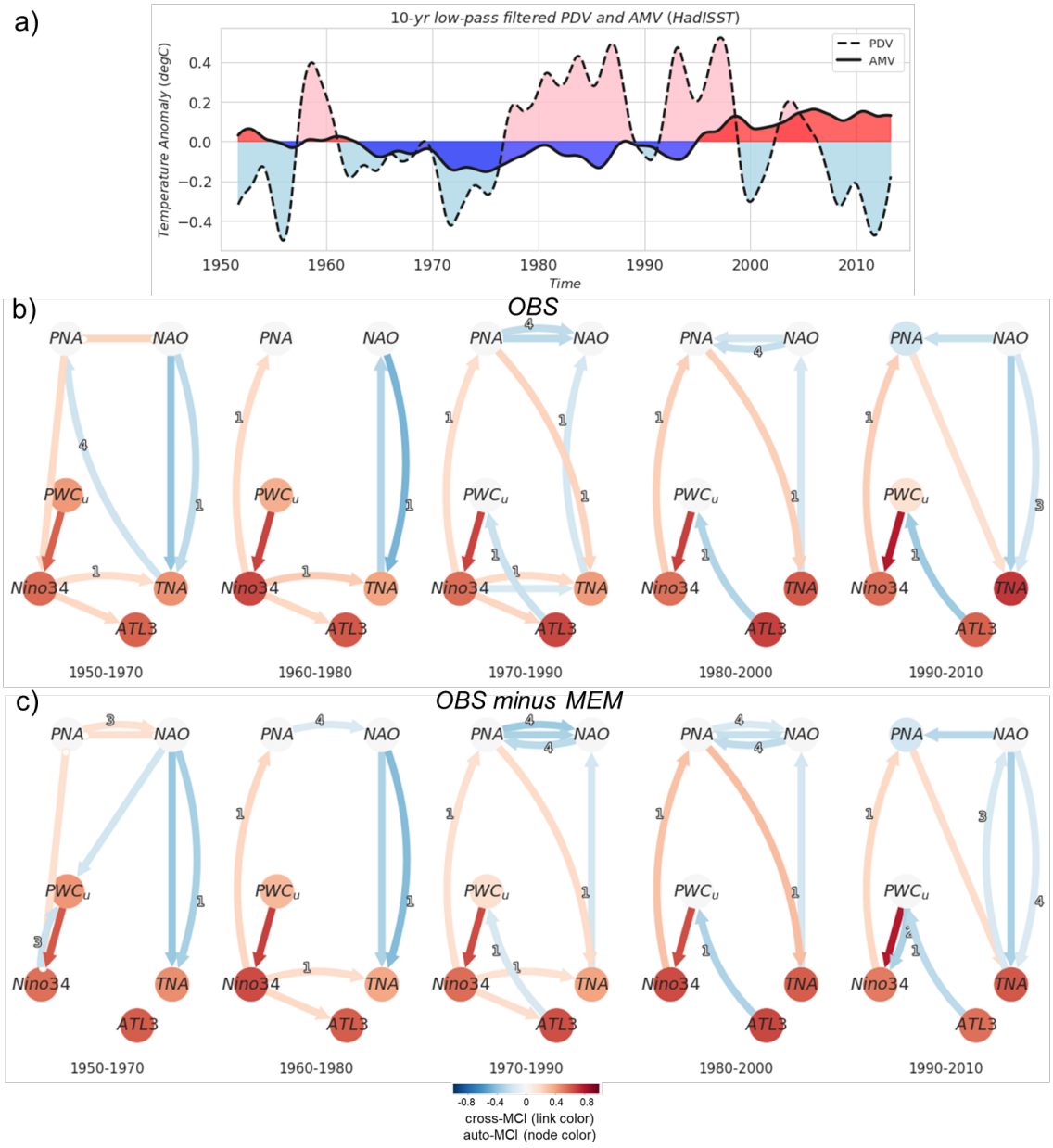

Figure 3. Observed Atlantic-Pacific interactions. a) 10-year low pass-filtered AMV (solid) and PDV (dashed) from the HadISST dataset, calculated following the definition in Sect. 2.4. b) Sliding window analysis where PCMCI+ is applied for five 20-year windows moving by 10 years (see subtitles for each causal graph). In this panel (b, OBS), the algorithm is run on the original time series before removing MEM. The link-associated time lags (unit=1 season i.e 3 months) are shown as small labels on the curved links. c) Similar to (b) but using data where the MEM is removed (OBS minus MEM).

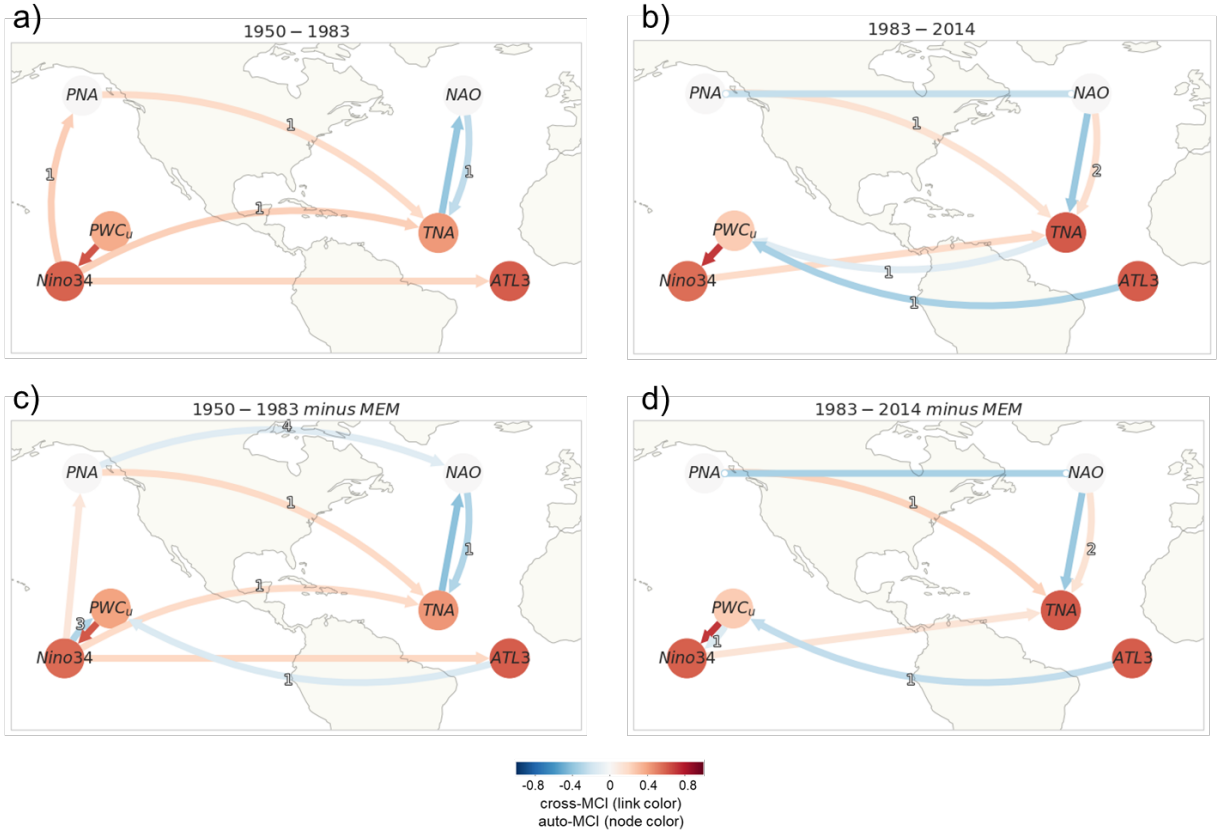

Figure 4. ~~Causal networks representing Atlantic-Pacific teleconnections for 1950-1983 (left column) vs 1985-2014 (right column) in the Reanalyses datasets. (a) Constructed by applying PCMCI+ on the standardized time series of the five seasonally averaged indices calculated from reanalysis datasets for the 1950-1983 period. Nodes represent the time series associated with each climate variability index (see node labels). Node colors indicate the auto-link coefficients (auto-coeff), and the color of the links denote the linear link coefficient (link coeff). The link-associated time lags (unit=1 season) are shown as small labels on the curved links. Straight links show contemporaneous inter-dependencies that happen with no time lag. (b) Same as (a) but for the 1985-2014 period. (c) same as (a), but with indices calculated after removing MEM. (d) Same as (c) but for the 1985-2014 period.~~Causal networks representing Atlantic-Pacific teleconnections for 1950-1983 (left column) vs 1983-2014 (right column) in the Reanalyses datasets. (a) Constructed by applying PCMCI+ the 1950-1983 period on the original time series before removing MEM. (b) Same as (a) but for the 1983-2014 period. (c) same as (a), but with indices calculated after removing MEM. (d) Same as (c) but for the 1983-2014 period.

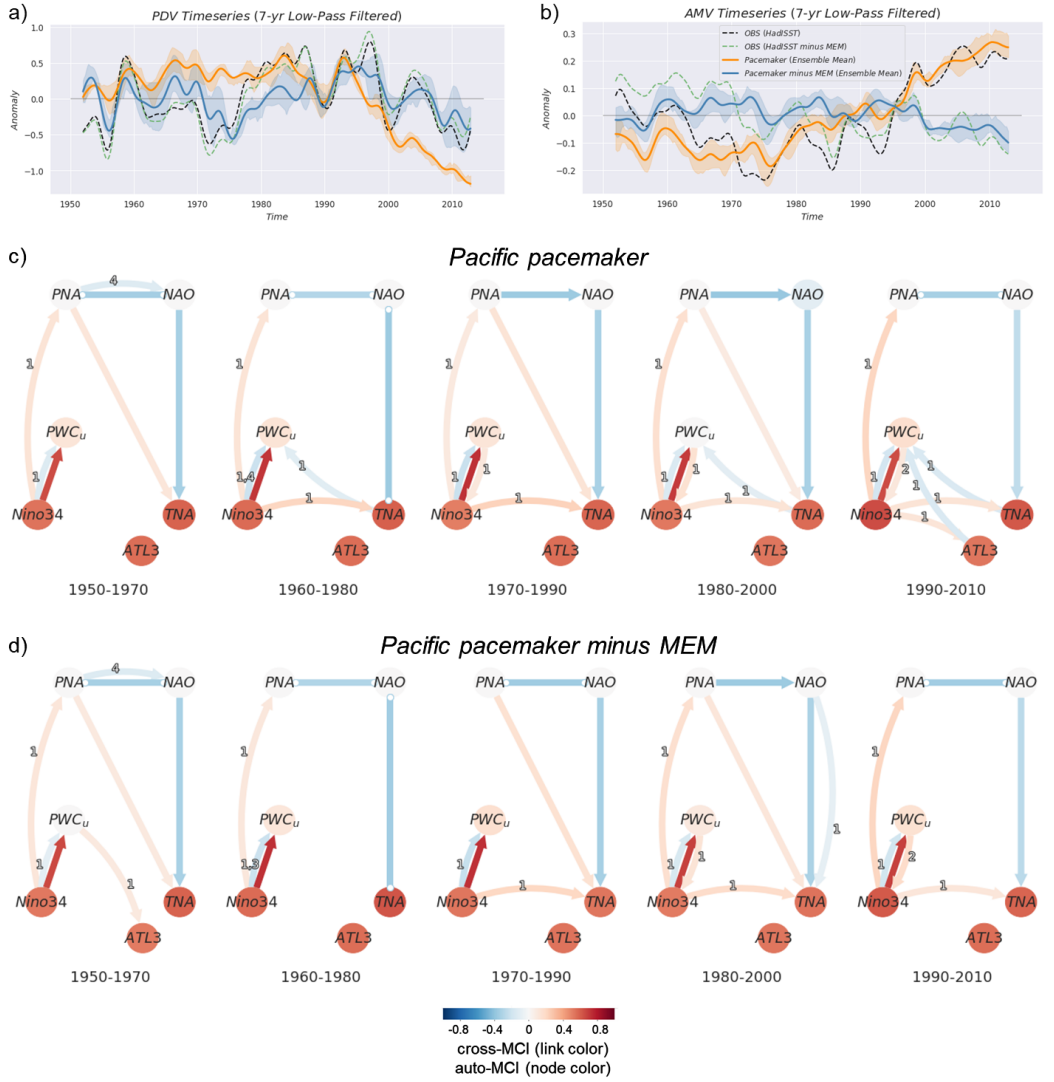

Figure 5. ~~Ensemble summary causal networks and time series from Pacific pacemaker simulations (1950-1983 vs 1985-2014). In panels (a-d), we apply the PCMCI+ on the time series of each simulation before aggregating the 10 causal networks into one. The link width shows the number of simulations that feature that link. The link color shows the mean value of link coefficients averaged over the ensemble members. The node color translates the average auto-coefficient of each time series among the pacemaker ensemble. The link labels provide the median time latency (rounded to the closest integer) for all ensemble members that detect a particular link. In (c) and (d) the MEM is subtracted from every simulation before PCMCI+ is applied. The average (auto-) coefficients were calculated after applying a Fisher z transform. The link labels provide the median time latency (rounded to the closest integer) for all ensemble members that detect a particular link.~~ Pacific pacemaker simulations where tropical Pacific SSTAs have been nudged toward observations (see Sect. 2.2). a) Pacific pacemaker ensemble average of the 7-year (Lanczos) low-pass filtered PDV time series (10 members) together with observations (HadISST, see legend in next panel) following definition in Sect. 2.4 for the 1950-2014 period. Solid lines denote the pacemaker ensemble-averaged time series before (orange) and after (blue) subtracting MEM. Shadings show the ensemble's 25th-75th percentile range. Dashed lines are for the same index calculated from the HadISST dataset before (black) and after subtracting MEM (green). b) Same as (a) but showing the AMV index. c) Same as Fig. 3b but using the Multidata-PCMCI+ function. Here, every window (see subtitle under each graph) shows a single causal graph representing the dependencies estimated from combined samples taken from all 10 pacemaker simulations. d) Same as (c) but for indices calculated after MEM is removed

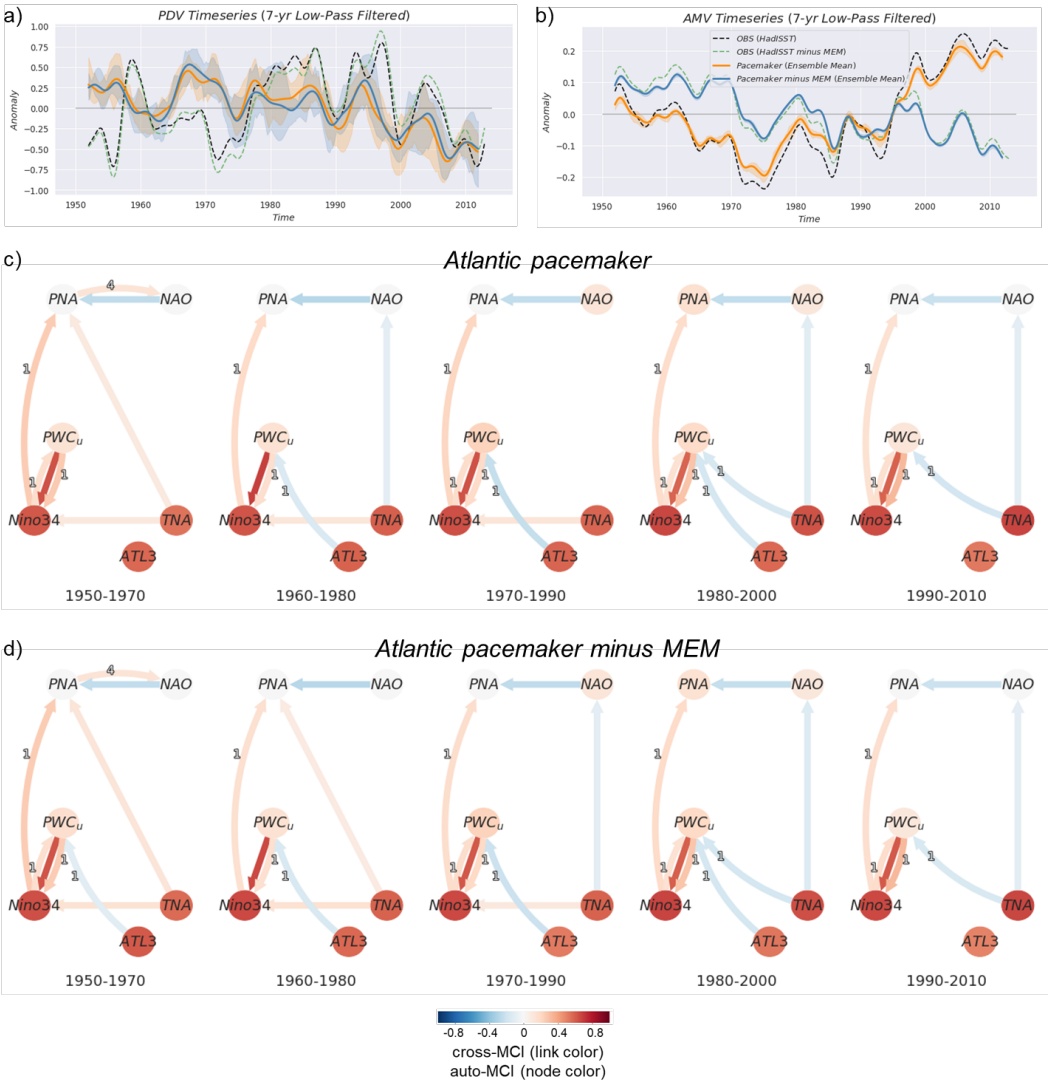

Figure 6. Atlantic pacemaker simulations where North Atlantic SSTAs have been nudged toward observations (see Sect. 2.2). Panels a-d here are similar to Fig. 5a-d but for the Atlantic pacemaker ensemble.

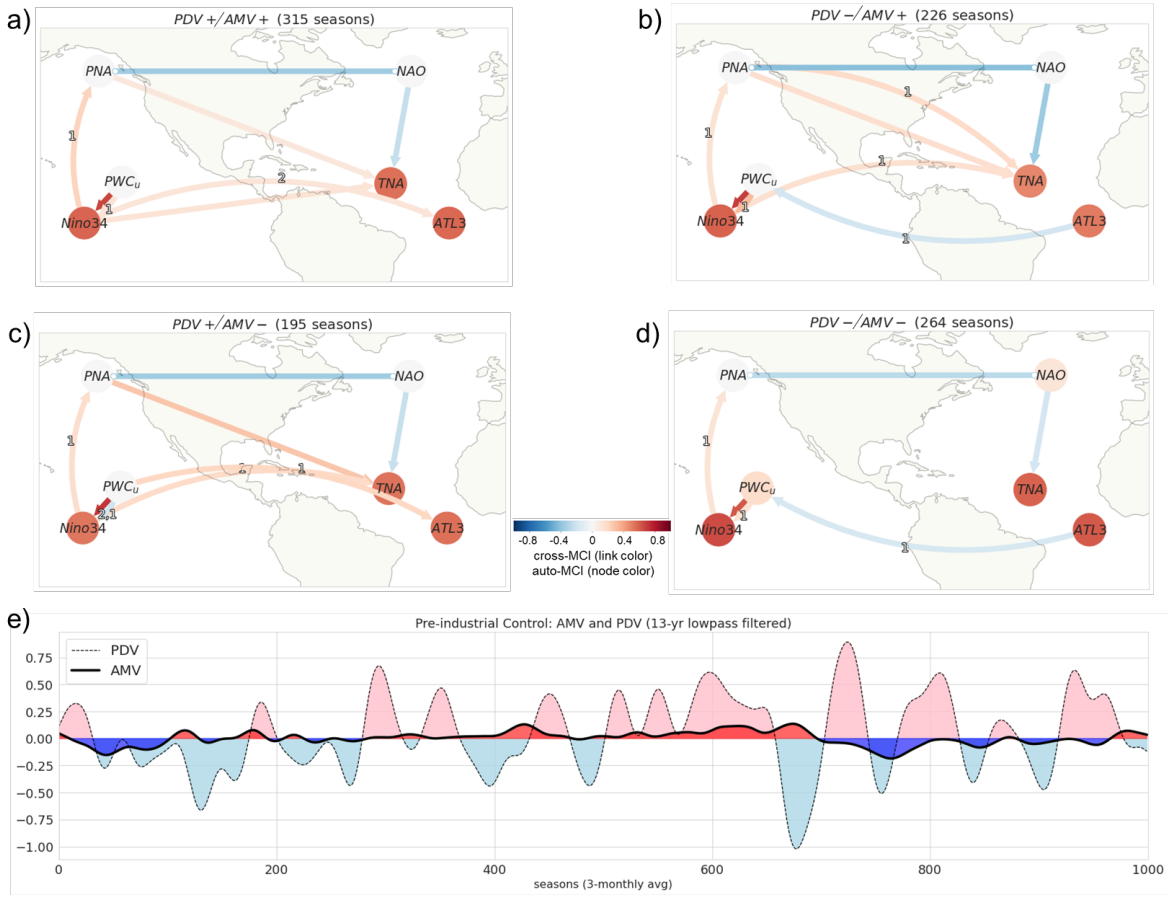

Figure 7. ~~CESM2 pre-industrial control simulation. a) Smoothed AMV and PDV indices (10-year low-pass filtered) illustrating the decadal internal variability over the Atlantic and Pacific for 120 years (480 time steps seasons). We divide the time series into three 40-year periods (labelled P1, P2 and P3; 160 seasons each), which express different states of AMV and PDV. b) For every period (P1-3) selected in panel (a), we show the respective causal network, similar to reanalysis data (Fig. 5) and pacemaker simulations (Fig. 7).~~ Regime-oriented PCMCI+ analysis of the CESM2 pre-industrial control run. a) Causal graph where only time steps corresponding to either a) PDV+/AMV+, b) PDV-/AMV+, c) PDV+/AMV-, d) PDV-/AMV- regime are considered. The regimes are defined according to the phase of e) smoothed AMV and PDV indices (13-year low-pass filtered) illustrating the decadal internal variability over the Atlantic and Pacific for 250 years (1000 time steps [seasons (3-monthly averages)]. Positive (negative) phases are shaded in pink (light blue) and red (blue) for PDV and AMV, respectively.)